UNIVERSITY OF CALIFORNIA SAN DIEGO

Understanding Non-coding haplotype effects via iPSC Endothelial Disease modeling

A dissertation submitted in partial satisfaction of the requirements for the degree
Doctor of Philosophy

in

Bioengineering

by

Evan L. Teng

Committee in charge:

Professor Adam J. Engler, Chair
Professor Pedro Cabrales
Professor Shu Chien
Professor Karen Christman
Professor John Shyy

2021

The Dissertation of Evan L. Teng is approved, and it is acceptable in quality and form for publication on microfilm and electronically.

University of California San Diego

2021

DEDICATION

To my mother and father

TABLE OF CONTENTS

LIST OF FIGURES

ACKNOWLEDGEMENTS

I would like to thank Professor Adam Engler for guiding me through the doctoral process and being a scientific mentor. The patience and understanding you have given me through my failures and successes has been one of the stabilizing pillars through my time in graduate career that I hope to exemplify in the future. I am also thankful to the rest of my committee – Professors Pedro Cabrales, Shu Chien, Karen Christman, and John Shyy – for their guidance through this process. In addition, I would like to thank my funding source through the National Institute of Health (NIH) T32HL105373 grant as this work would not be possible without this assistance.

I would like to thank the Engler Lab as a whole for helping shape my research and myself positively over the years. In particularly, I'd like to thank Aditya Kumar for being a fun and helpful graduate mentor, helping to get me started on this research, and being a good friend. I am especially grateful for my undergraduate students – Brenda Ngo, Jessica Fung, and Rachel Liang – for shouldering the work I could never do alone and supporting me through the ups and downs of research. I hope to continue to support your aspirations as well in the future, regardless of where life takes you.

Lastly, I would like to thank my family and all the friends that have supported me through these years. My time spent with all of you has taught me so much and given me so many memories that I continue to cherish to this day. To my mother and father and sister: thank you for always supporting me in every way. I would not be where I am today without you, and for that I am eternally grateful. I hope I have made you proud.

Chapter 1, in full, is a modification of the material as it appears in: Teng EL, Engler AJ. 2017. Mechanical influences on cardiovascular differentiation and disease

modeling. *Experimental Cell Research*. https://doi.org/10.1016/j.yexcr.2019.02.019. The dissertation author was the primary author of this paper.

Chapter 2, in full, is a modification of the material as it appears in Teng EL, Masutani EM, Fung J, Lian R, Ngo B, Kumar A, Placone JK, LoSardo V, Engler AJ. High Shear Stress enhances Endothelial Permeability in the presence of the Risk Haplotype at 9p21.3. *APL Bioengineering.* In Review. The dissertation author was the primary author of this paper.

VITA

2015 Bachelor of Science, Georgia Institute of Technology

2021 Doctor of Philosophy, University of California San Diego

PUBLICATIONS

Teng EL, Masutani EM, Fung J, Lian R, Ngo B, Kumar A, Placone JK, LoSardo V, Engler AJ. High Shear Stress enhances Endothelial Permeability in the presence of the Risk Haplotype at 9p21.3. *APL Bioengineering, 2021.* In Review

Teng EL, Engler A. 2017. Mechanical influences on cardiovascular differentiation and disease modeling. *Experimental Cell Research*. 377, 103-108 https://doi.org/10.1016/j.yexcr.2019.02.019

Lo Sardo V, Chubukov P, Ferguson W, Kumar A, **Teng E**, Duran M, Zhang L, Cost G, Engler A, Urnov F, Topol E, Torkamani A, Baldwin K. 2018. Unveiling the Role of the Most Impactful Cardiovascular Risk Locus Through Haplotype Editing. *Cell*. 175:1796-1810. https://doi.org/10.1016/j.cell.2018.11.014

ABSTRACT OF THE DISSERTATION

Understanding Non-coding haplotype effects via iPSC Endothelial Disease modeling

by

Evan L. Teng

Doctor of Philosophy in Bioengineering

University of California San Diego, 2021

Professor Adam J. Engler, Chair

The mechanical forces surrounding cells can have far reaching influences on cellular function. In particular, differentiation of stem cells into the cardiovascular lineages can be impacted by numerous environmental factors, including stiffness of surrounding ECM, stretch or strain on cellular attachment, and contraction of the cells themselves. However, the cardiovascular lineage cells themselves induce mechanical forces on their surroundings as well, notably with regards to cardiomyocyte or smooth

muscle cell contraction. In combination with induced pluripotent stem cells and the use of genetic modifications, studying the connection of mechanical function to disease risk genetics can be well documented in vitro. In looking into how the cardiovascular 9p21 risk haplotype influences smooth muscle cells, we found iPSC-derived SMCs with homozygous risk (R/R) haplotype were found to have lower cellular adhesion as well as global contractility through spinning disk shear and collagen gel contractility assays, respectively.

We then examined how the 9p21 risk haplotype influences endothelial cell function in relation to coronary artery disease. In a static environment, iPSC-derived ECs of R/R haplotype exhibited greater permeability and showed greater reactive oxygen species generation compared to knockout (KO) and non-risk (N/N) haplotypes. In the presence of inflammatory cytokine TNFα, EC monolayers showed greater permeability independent of haplotype. However when grown in a 3D microvessel environment with pathological wall shear stress levels, R/R ECs showed greater permeability and vessel wall detachment. The genomic expression of these R/R ECs also displayed decreased EC adhesion genes and ECM genes but also a reversal into greater CAD associated transcriptomic expression compared to static conditions as established by a subset of previously identified CAD risk genes. These data suggests the presence of pathological shear stress may regulate the 9p21.3 non-coding risk loci in the context of CAD.

While the research detailed here applies to cardiovascular disease in particular, the concepts behind cellular mechanics and their surroundings are far reaching, applying to other diseases and homeostatic conditions. The use of 3D microfluidic vessel

formation and application of in vitro fluidic shear modeling is a tool that can hopefully be applied to further human disease ailments and research in the future.

Chapter 1.

Mechanical Influences on Cardiovascular Differentiation and Disease Modeling

1.1 Abstract

Tissues are continuously exposed to forces in vivo, whether from fluid pressure in an artery from our blood or compressive forces on joints from our body weight. The forces that cells are exposed to arise almost immediately after conception; it is therefore important to understand how forces shape stem cell differentiation into lineage committed cells, how they help organize cells into tissues, and how forces can cause or exacerbate disease. No tissue is exempt, but cardiovascular tissues in particular are exposed to these forces. While animal models have been used extensively in the past, there is growing recognition of their limitations when modeling disease complexity or human genetics. In this mini review, we summarize current understanding of the mechanical influences on the differentiation of cardiovascular progeny, how the transduction of forces influence the onset of disease, and how engineering approaches applied to this problem have yielded systems that create mature-like human tissues in vitro in which to assess the impact of disease on cell function.

1.2 Introduction

When first identified and then isolated nearly two decades ago, the promise of embryonic stem cells rested in their regenerative potential, to assist the body where natural processes either incompletely as with scarring or completely as in heart disease failed to maintain or regenerate function. With their ability to differentiate into many specific cell types, a vast number of chronic diseases were thought to have a new therapeutic option. While expectations have been significantly tempered since then, due to safety and efficiency concerns among others, their ability to mirror complex disease in vitro, especially when patient-specific genetics (using induced pluripotent stem cells or iPSCs) and appropriate unique environmental conditions are present, has provided a new avenue of research over the past several years with relatively easy entrance into the field. For example, iPSCs can now be created from easily accessible cell types such as fibroblasts, keratinocytes, and peripheral blood mononuclear cells and numerous companies and core facilities are available to create patient-specific lines for researchers. However, the challenge remains with a second caveat that an appropriate cellular environment should be present to ensure appropriate differentiation and separately to model disease-in-a-dish (1). Without these conditions, differentiation efficiency and purity may be lower and specific disease-like behaviors may not occur (2). As such, we focus this mini review on a summary of the state-of-the-art in modeling diseases-in-a-dish (1, 3), first examining how the surrounding niche and its mechanical properties have been used to optimize differentiation and secondly to induce disease-specific conditions and monitor cell outcomes.

1.3 Mechanical Influences on Stem Cell Differentiation into Cardiovascular Lineages

Many recent investigations have taken advantage of our current understanding of developmental biology to create protocols for specific cell type differentiation, including cardiovascular progeny such as cardiomyocytes (4), endothelial cells (ECs) (5), and smooth muscle cells (SMCs) (5). These protocols typically involve the addition of certain key growth factors added to stem cell media to take advantage of the biological and chemical cues involved in embryogenesis to induce mesendoderm differentiation pathways. Differentiation protocols range in duration from weeks to months, depending on cell types. Given that cardiovascular cells have common progenitors (6), purifying techniques including cell sorting and selection media are often necessary to ensure high purity. While typically highly defined, protocols can also involve 3D culture as embryoid bodies (EBs) (7) or in 2D on tissue culture plates coated with Matrigel or other matrix ligands (8) to create cardiovascular progeny. However while stem cells respond to numerous environmental factors, recent evidence has suggested that physical parameters are as important as the chemical ones that have been described above (9, 10). For reference, we have summarized the common differentiation stages and the markers that describe them in Figure 1 from references (4-8) noting that this is not an exhaustive list either in terms of stages or markers (shown in red). We also include, as known, a summary of where mechanical cues, be they active or passive, influence differentiation for each lineage and the maintenance of PSC/iPSC self-renewal (indicated by blue numbers corresponding to specific mechanical cues in the dashed box). As described

below, mechanical cues are often applied throughout differentiation such that they are not specific to a given stage, applied to culture conditions where their influence is less direct, e.g. multicellular EBs, or applied to further enhance chemically defined protocols at their conclusion or to alter the phenotype of a committed cell.

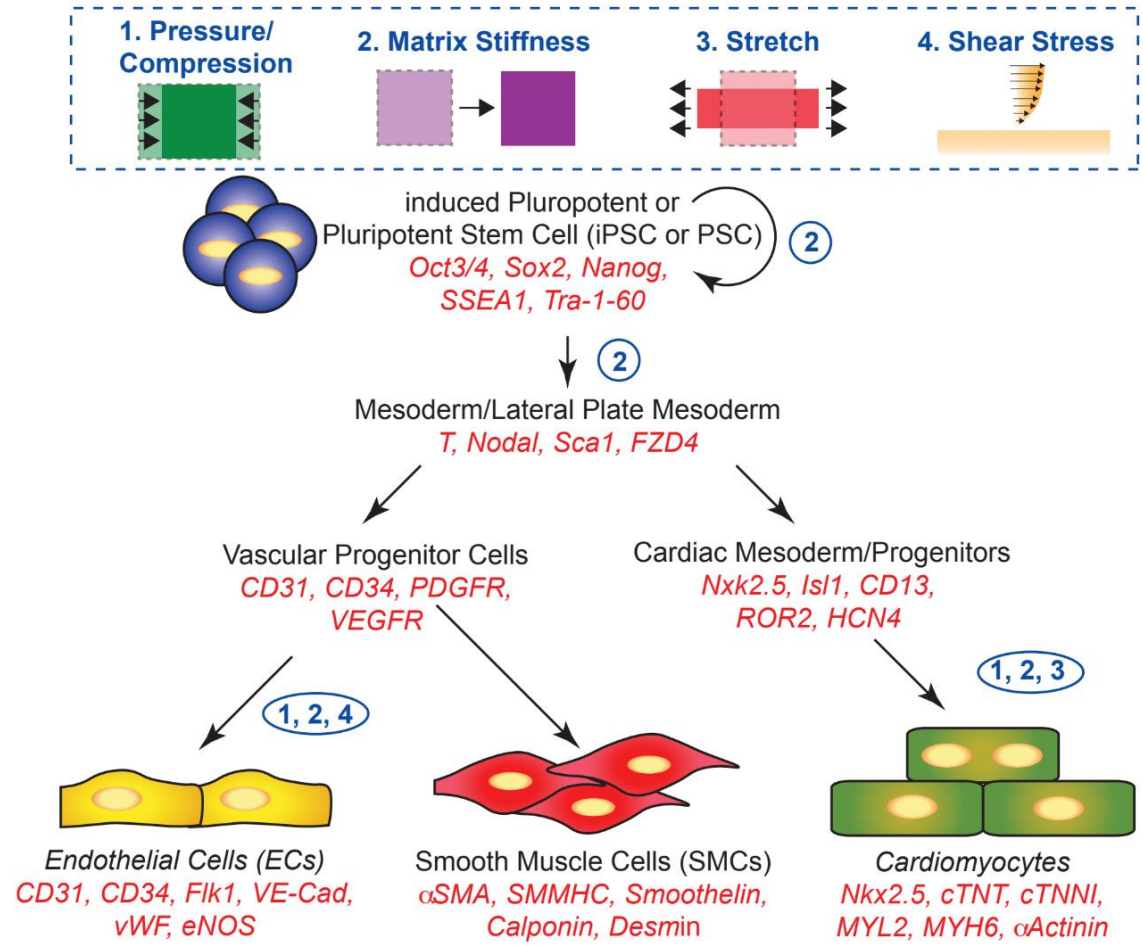

Figure 1.1. Mechanical Influences on Cardiovascular Progeny
This Schematic depicts stem cells and their key progenitor stages during chemically mediated differentiation protocols; black arrows denote cells' progression through the differentiation process (circular arrow at top denotes self-renewal). Red italics indicate genes characteristic of each stage. Mechanical cues and/or signals are shown in the blue box (top) and circled numbers by each arrow indicate the differentiation stage at which each can have an effect.

1.3.1 Mechanical stimulation and maturation on cardiomyctes

Concurrent with growth factor-driven primitive heart field specification through mesoderm induction and cardiac specification, significant changes in mechanics, both

matrix deposition and pressure changes (11), drive progenitor cell fate in the early heart in vivo. Subsequently mechanical demands can change frequency- and length-dependent contractility, allowing the mature tissue to accommodate beat-to-beat variability as organism activity changes. Active mechanical stretch, when integrated into differentiation protocols, however, may be dose and context specific (12-14). Since beneficial conditions have been less chemically defined, others have examined the influence of passive properties, such as stiffness of the culture substrate, or when these material properties are varied in space or time. In a small range of substrate stiffness that is developmentally appropriate for the heart, nascent cardiac muscle organizes itself better (15, 16). More recently, dynamic changes in the substrate, which better mirror developmental changes in matrix (11), have been shown to further improve specification of pre-cardiac mesoderm (17). Despite all of these inductive cues, a chronic problem with cardiomyocytes is their inability to induce functionally mature cells from PSCs or iPSCs, i.e. they are unable to replicate phenotypic and mechanistic characteristics of primary tissue. To combat this maturation problem, it is becoming increasingly popular to differentiate cells in chemically defined cultures for 60+ days (4), and, once at the immature cardiomyocyte stage, to add external stimuli to further enhance maturation. For example, functionally mature cells form gap junctions allowing for the electrical connections between cells, and when exposed to 10% cyclic stretch, immature cells form more robust junctions (18). Equally common are studies that explore myofibrillogenesis in immature or neonatal cardiomyocytes where mechanical influences drive the assembly of the contractile apparatus (15, 16). It is important, however, to note that cell origins

with these studies are not always PSCs and thus should only be seen as separate from those mentioned above that look at de novo influences of mechanics on stem cells.

1.3.2 Mechanical forces on endothelial and smooth muscle cells

In addition to influences on cardiac specification, differentiation, and maturation, vascular progeny are also influenced by mechanical stimuli. Endothelial cells, which line the vessel wall, are a perfect example of these effects. Pluripotent stem cells (PSCs) or their endothelial progenitor cells (EPCs) can take on mature characteristics when placed under physiological shear stress (19). While additional purification by fluorescence activated cell sorting is required, it is important to note that unlike cardiomyocytes, mechanically-mediated signaling is an important component of EC differentiation in chemically defined conditions, so long as shear remains physiological; under normal flow of 10-20 dynes/cm^2, shear stress is felt by the cytoskeleton as an 'outside-in' signal (19-22). However when flow becomes pathological in magnitude or disturbed (i.e. not laminar), differentiation of progenitors and critical functions of mature endothelial cells, e.g. tight junction maintenance, become compromised. For example, iPSC-derived microvascular endothelial cells form tight junctions (23), but upon exposure to increasing flow, junctions remodel and EC monolayers become more permeable (21, 24). Underlying these changes are mechanosensory complexes, which are also implicated in controlling progenitor maturation (25). Thus when aberrant flow is present in the developing embryo or in microphysiological systems meant to recapitulate differentiation conditions, cells fail to completely mature. While ECs are typically differentiated from iPSCs or PSCs (5) for disease modeling, vessel lumens constantly turn over in vivo, in which case they are created from EPCs. These cells, which are recruited from bone

marrow into peripheral blood, circulate and attach to the existing endothelial lumen, transmigrate, and then replace, repair, or create neo-vessels; luminal damage, due in part to excessive shear stress or disturbed flow (21), recruit EPCs, and evidence suggests that as they home to the injury site, EPCs become mechanosensitive (26); after adhering to the lumen, EPCs upregulate canonical EC markers and reinforce cell-cell and cell-matrix adhesive structures in a shear stress-dependent manner in order to transmigrate (20). Whether arising from PSCs or EPCs, EC differentiation is also sensitive to stretch, as in vivo vessels are constantly stretched from cyclic changes in pressure (21). While its effects are less clear for ECs, mechanisms at the cell membrane most likely differentiate between mechanical inputs and determine the differentiation pathways to be activated. Aside from shear stress, other mechanical cues, including passive matrix stiffness (22, 27), compression (28), and vessel pressure (9) also contribute to final EC specification but evidence of its specific influence at progenitor stages is not clear to date.

Along with ECs, SMCs are also mechanically active vascular cells that are clearly involved in many disease processes. There is extensive literature on chemically defined differentiation protocols to create SMCs from iPSCs (5) and adult stem cells (29) based on developmental pathways (30), but the effects of mechanics on their differentiation from iPSCs or PSCs is less certain. Significant effort in mechanics has been focused on its effects on adult stem cells, e.g. alignment relative to the stretch axis, although a variety of disparate effects have been observed, e.g. perpendicular or parallel alignment, increased SMC gene expression, etc. (29). Significant effort has also focused on phenotype plasticity once committed to the SMC lineage (hence the mechanical cues noted in Figure 1 do not point to SMC differentiation pathways). This latter focus is due

in part to significant changes that SMCs can make in the medial layer of the vessel, which causes them to invade the tunica intima, form plaques, and alter local hemodynamics. As such, we will leave the majority of our discussion of mechanical influences on SMCs for subsequent sections on the impact of disease and the use of iPSCs for disease modeling.

1.4 Disease-mediated mechanotransduction as a basis for in vitro modeling

Mechanics influences nearly every major solid organ and its disease processes, but central to most cardiovascular diseases is altered transduction of signals within or between cells or layers of cells; these signals can alter cell phenotypes to exacerbate disease outcomes. As the cardiovascular field has known over more than two decades, ECs and SMCs are able to maintain physiological homeostasis by reciprocally modulating barrier function via junctions and vessel tone via contracting (21, 31). Indeed, vessels and the heart wall are elastic and capable of dynamically responding to physiological changes in the microenvironment, e.g. variations in shear stress from blood flow (10-20 dynes/cm^2), arterial pressure up to ~20 kiloPascal, and artery wall strains up to ~100 kiloPascal (32). Should mechanical input begin to fall outside of the range where cooperative mechanical signals–either direct or indirect–can adjust cell function, cells plastically change phenotype, which can induce disease (9, 10, 31, 32). Atherosclerotic plaque formation is one such example where disturbed flow can cause oxidative stresses and lipoprotein accumulation in ECs, inflammatory cells then home to the site whereupon they take up the lipoprotein and become foam cells, and finally SMCs are recruited to

form a fibrous cap on the plaque (33). For each of these cell types, mechanical signals help in part to recruit cells involved or to create conditions that caused phenotypes to change. One classic example at the cellular level is SMC phenotype; although a relatively small fraction that contributes plaque formation in vivo (34), significant evidence in vitro describes conditions where excessive stretch, compression, and shear will transform SMCs from ‘contractile’ to ‘synthetic’ via changes in morphology, proliferation, migration, and marker protein expression (35). While some heterogeneity can be beneficial, it is clear that plaque formation among many diseases induce permanent phenotype changes in vascular cells that are detrimental to function.

1.4.1 Multi-cellular roles in cardiac injury

While vessels highlight crosstalk between vascular cell types, cardiomyocyte contributions to heart disease in the myocardium highlight crosstalk between pathways within a cell. Multiple intra- and extra-cardiomyocyte structures, e.g. sarcomeres, intercalated discs, and the extracellular matrix, remodel during disease progression and contribute to pathology to varying degrees. Within each of these structures, multiple protein complexes have been identified (36), but their specific contributions to disease are uncertain; for our purposes however, it is perhaps more helpful to consider the functional consequences that can subsequently be modeled in vitro. For the sarcomere, which serves as point of contractile force generation in cells, mutations disrupt assembly and attenuate contractility. Mutations in titin for example, a protein that helps set sarcomere length, cause dilated cardiomyopathy by impairing sarcomere formation (37) and alignment (36). For intercalated discs, which electrically connect myocytes together, defects arising from missing components such as the connexins impair conduction and

can cause arrhythmogenic cardiomyopathies (38). Beyond specific mutations, cardiomyocyte hypertrophy, i.e. an increase in cell size, enhances protein synthesis, heightens organization of the sarcomere, but can also lead to specific dysfunction within the myocyte (39). While these examples focus inside the myocyte, mechanical transductive defects across the heart wall itself, such as wall strain, influence not only lineage commitment (12, 13, 18) but also contribute to cardiomyopathies when excessive (40). This can activate other myocardial cells, including cardiac fibroblasts, via signals transduced by extracellular matrix. These cardiac fibroblasts, in the event of cardiac dysfunction, begin to secrete ECM proteins, resulting in a stiffening of the localized cardiac injury. Such matrix deposition and remodeling, while possibly salvaging mechanical functionality temporarily, ultimately alters the heart wall mechanical flexibility and stiffness. An increase in mechanical stiffness has multiple negative consequences for the myocardial cell population. Increases in myofibroblast populations of fibroblast lineage increases further matrix deposition, cell motility, and inflammatory signaling such as TNFalpha. The increase in inflammatory signaling recruits more macrophages to the sight of injury which they themselves increase additional inflammatory cytokine release, perpetuating a chronic inflammation cycle. The increase of surrounding stiffness further leads to cardiac dysfunction, such as hypetrophy, as well as increased contraction stress by cardiomyocytes. Thus, while we focus on myocytes specifically, other cell types within the heart play a role in disease progression.

1.5 Improvements on Disease Modeling with iPSCs and Mechanics

While mammalian models are closely related to the human condition, there remain key genetic and physiological differences between human and mammalian models, particularly mouse and rat models. For specific genetic questions involving mechanotransduction like those raised above, mammalian systems are inappropriate or fail to recapitulate key hallmarks of human disease (41, 42). Cadaveric models or primary human cells could be ideal in this situation, but many cell types and systems are difficult to study by the nature of those cell types lacking proliferative phenotypes or source acquiring difficulty, such as cardiac, endothelial, and neural tissue. Thus instead of acting in a confirmatory manner, iPSC- or PSC-derived cell types are therefore a highly plausible option to investigate these systems and cell types as a reliable and consistent source for in vitro modeling and small scale drug testing.

1.5.1 Induced PSCs in targeted disease-in-a-dish models

Patient-specific iPSCs in particular are becoming more accessible and provide a steady source of *in vitro* human cells. They have become a standard means of modeling the genetic underpinnings of disease-in-a-dish (3) with minimal concern for patient variability, reprogramming vector, and differentiation protocol heterogeneity that existed even a few years ago (43, 44). Recent technological advances in the ease of iPSC derivation, in cardiovascular differentiation protocols (4, 5), and in relatively straightforward genome editing techniques (45) enable one to insert or delete patient-specific variants and create standard, reproducible, and isogenic models. Gene editing techniques now even allow knocking in or out mutations over a range up to several thousand kilobases. This can enable isogenic comparison between two cell lines of the same cell type, providing a statistical comparison difficult to create otherwise. Using this

methodology, the field has developed significant understanding about how mutations affect signaling (46) and cytoskeletal architecture (1, 3, 36, 37) in the progression of heart disease. Despite these advances in both technology and understanding of cardiovascular disease, new concerns have arisen about how widely applicable disease-in-a-dish models may be.

1.5.2 Concerns of current disease-in-a-dish models

One current concern raised with the disease-in-a-dish strategy is that the models typically developed now employ monocultures. While many differentiation protocols today aim to achieve as pure and mature a population as possible (4, 5), realistically, there is significant heterogeneity within a complex structure such as the endothelium, vessel, or myocardium, even within a single cell phenotype (35); single populations are simply less representative. Complex diseases described above cannot arise when crosstalk is needed if only one cell type is present. The beneficial effects of co-culture models have been observed in organoids, so similar combinations in vessel or heart wall models may not be as technically challenging as one might expect. While appropriate tissue striation may not be apparent, initial attempts at multi-lineage cardiovascular tissues indicate some degree of mimicry with human tissue, at least in terms of assessing drug toxicity (47).

A second concern–and one directly applicable to mechanics–is the lack of 3D structure and context specific forces in many current disease models (1-3, 36, 37, 46); 2D substrates in static cultures remain all too common (2). Spatial complexity in disease modeling is necessary for understanding of propagational effects across tissue such as mechanical contraction and full construct deformation, disease-response signaling of co-

culture in relation to spatial positions and motility of involved cells, and electrical conduction and impedence through sections rather than a sheet of tissue. Bioengineering efforts have attempted to begin addressing this using a variety of systems, including material-patterned cell rings (i.e. “tissue rings”) (48), 3D meshes of many types and synthesis methods (49, 50), degradable natural or synthetic materials (51-55), and self-

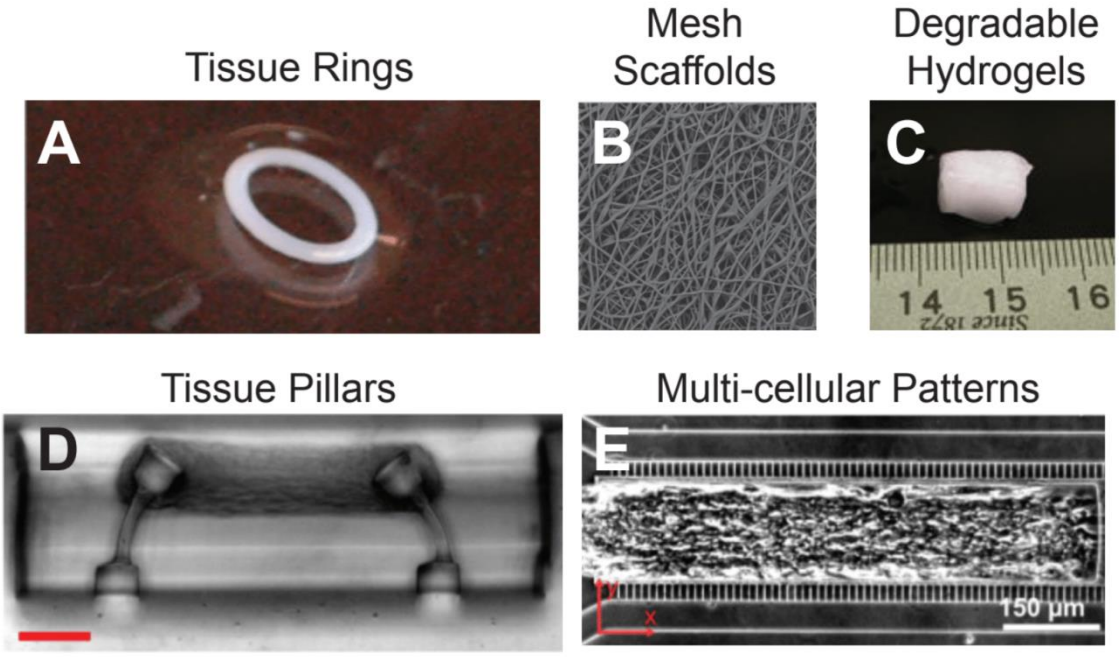

assembled multicellular structures (i.e. “tissue pillars”) (56-58) among others. Specifically when using iPSC-derived progeny to create microphysiological systems,

Figure 1.2. Mechanical active disease models in a dish
Images illustrate the breadth of fabrication methods employing bioengineering approaches to create systems that mimic cardiovascular mechanics in vitro to better model disease. Specifically labs have created tissue rings where embedded cells contract a matrix polymerized around a central post resulting in a tissue ring (A) , electrospun scaffolds where cells migrate throughout the material to create a 3D tissue (B), polymerized hydrogels with cells embedded in it (C), embedded cells in a matrix that are allowed to contract around multiple posts and is often flexible to report contractile force (D), or created chambers where multicellular tissues are exposed to controlled flow (E). Images are reproduced from references [48], [50], [55], [56], and [62], respectively.

however, groups have emphasized the need to develop dynamic systems (59) that reproduce critical aspects of in vivo physiology (60) and electrical conduction (61).

Additional effects of external mechanical stimuli on 3D structure is an area in need of further investigation. When iPSC-derived cells from genetically characterized diseased patients are used, influence from the genotype should be readily apparent. Similarly, drug responses should reproducibly alter the system's physiology as well (58, 62). Figure 2 provides a summary of common approaches to building in vitro structures that better model disease.

Along with the need to increase the mechanical complexity of the niche in 3D to better model disease, it is important to note that these systems remain relatively small as they rely primarily on diffusion for nutrient transport. While an engineered vasculature would directly address this third concern, the efforts described above remain focused on constructing larger vessels that could be scaled down. Similarly the engineering challenging of scaling up to larger and more interconnected systems remains largely unsolved. Thus the success of future attempts at disease modeling and understanding disease mechanisms using in vitro systems hinges on solving these concerns.

1.6 Conclusion

Stem cells are a promising technology with the potential to be utilized at the bedside in addition to their current role in the lab. New clinical trials continue to investigate how stem cells can be used. Yet given the experiment challenges that are ahead, stem cells remain an excellent tool to investigate difficult to attain human tissue, model disease and genetic conditions, and observe phenotypic changes, e.g. smooth muscle transition from contractile to synthetic. However, one must be aware that while stem cells offer much flexibility and ease of acquisition in comparison to some human

tissue samples, the concern of tissue maturity and complexity remains present in studies involving stem cells. With additional advancement in stem cell culture and differentiation technique, which could involve simultaneously biologically, chemically, and mechanical stimulation for differentiation, the perspective on stem cells as a promising clinical and investigative tool for understanding and treating human disease and genetic conditions continues to grow brighter.

1.7 Acknowledgements

The authors acknowledge support from National Institutes of Health (NIH) grants 2R01AG045428 (A.J.E.), T32HL105373 (E.L.T.) provided support for this work. National Science Foundation grant 1463689 (A.J.E.) also provided support.

Chapter 1, in full, is a modification of the material as it appears in: Teng EL, Engler AJ. 2017. Mechanical influences on cardiovascular differentiation and disease modeling. *Experimental Cell Research*. https://doi.org/10.1016/j.yexcr.2019.02.019. The dissertation author was the primary author of this paper.

Chapter 2.

High shear stress enhances endothelial permeability in the presence of the risk haplotype at 9p21.3

2.1 Abstract

Single nucleotide polymorphisms (SNPs) are exceedingly common in non-coding loci, and while they are significantly associated with a myriad of diseases, their specific impact on cellular dysfunction remains unclear. Here we show that when exposed to external stressors, the presence of risk SNPs in the 9p21.3 CAD risk locus increases endothelial monolayer and microvessel dysfunction. Endothelial cells (ECs) derived from induced pluripotent stem cells of patients carrying the risk haplotype (R/R WT) differentiated similarly to their non-risk (N/N) and isogenic knockout (R/R KO) counterparts. Monolayers exhibited greater permeability and reactive oxygen species signaling when the risk haplotype was present. Addition of the inflammatory cytokine TNFα further enhanced EC monolayer permeability but independent of risk haplotype; TNFα also did not substantially alter haplotype transcriptomes. Conversely when wall shear stress was applied to ECs in a microfluidic vessel, R/R WT vessels were more permeable at lower shear stresses than R/R KO vessels. Transcriptomes of sheared cells clustered more by risk haplotype than by patient or clone, resulting in significant

differential regulation of EC adhesion and ECM genes versus static conditions. A subset of previously identified CAD risk genes invert expression patterns in the presence of high shear concomitant with altered cell adhesion genes, vessel permeability, in the presence of the risk haplotype, suggesting that shear stress could be a regulator of non-coding loci with a key impact on CAD.

2.2 Introduction

Heart disease remains the leading cause of death in the United States (63), and in particular coronary artery disease (CAD) is the most prevalent form worldwide (64). While significant risk for CAD is associated with lifestyle, there is growing recognition that genetics has a profound influence on risk. Genome wide association studies (GWAS) have identified a number of single nucleotide polymorphisms (SNPs) within the 9p21.3 locus with extremely high correlation to increased risk of acquiring CAD and myocardial infarction (65, 66). This region contains an antisense noncoding RNA called *ANRIL (CDNK2B-AS1)* and borders the CDKN2A and CDKN2B genes (67, 68) whose function is not well understood. Notably, this particular locus is found only within close evolutionary relatives of humans, e.g., chimpanzees and Rhesus macaques; it is not found in commonly studied rodent species (42, 69), and hence orthologous knockout studies of the syntenic mouse region (41) yielded results with unclear human relevance. Given the challenges involved in human and primate research, patient-derived induced pluripotent stem cells (iPSCs) offer a suitable alternative means of interrogating the 9p21.3 CAD risk locus effects at the cellular level (70). Indeed, recent evidence suggests that the

haplotype's presence significantly impairs the function of iPSC-derived cardiovascular progeny (71, 72).

The process of CAD-associated injury and plaque buildup within arterial walls involves several different cell types (73), including resident endothelial cells and smooth muscle cells as well as immune response cells such as macrophages. With the presence of stressors within the blood, excessive tunica intima permeability from leaky tight junctions leads to fatty build up, expanded foam cell presence, and smooth muscle invasion, which decrease lumen area and restrict blood flow (74). While CAD progression is well studied, how this downward cascade of vessel health begins in relation to endothelial cell dysfunction is less understood. ECs reside in the innermost layer of the blood vessel, separating the lumen from the vessel wall and regulating nutrient and molecular transport beyond the vessel. In addition, ECs also are critical in mediating macrophage attachment and entry into the blood vessel via extravasation, which can exacerbate vessel injury (75). Like their cardiomyocyte counterparts (72), external factors–either chemical or physical–can influence how ECs are able to fulfill these functions (76). For example, EC barrier function is susceptible to inflammatory cytokines, notably TNFα and Interleukin 6 (IL-6) which are typically present in cases of injury and inflammation (77). Hemodynamic shear stress also influences EC function (76, 78). For example, laminar shear stress as well as low magnitude oscillatory flow is atheroprotective. However, disturbed or turbulent flow increases inflammation and cellular damage (79) which high, pathological shear stress can reverse beneficial effects due to increased blood parameters of pressure, flow, or vessel tightening (80).

The myriad of genetic, biochemical, and physical effects on ECs demonstrate a complex environment whose holistic effects are not fully understood. To better understand the role that the 9p21 region has on EC physiology and regulation of vessel integrity, we characterized iPSC-derived EC (5) morphology and function in the presence of the risk haplotype. To introduce fluidic stress effects into the equation, we built a 3D microfluidic device, comprised of an iPSC-derived EC microvessel within a collagen scaffold, and determined laminar shear effects on the EC microvessel, its permeability, and its structural integrity with relation to the 9p21 risk haplotype presence. These observations further suggest that interaction between the 9p21 risk locus and environmental stress represent a key factor in CAD onset and progression.

2.3 Results

2.3.1 9p21.3 CAD risk haplotype does not impair iPSC-EC differentiation

iPSCs carrying the homozygous risk haplotype (R/R assessed by genotyping at rs1333049, rs2383207, and r10757278), the knockout isogenic lines edited by TALENs (R/R KO), or those carrying the non-risk haplotype (N/N) (71) were verified for their pluripotency via staining of Sox2, Nanog, and Oct4 (**Fig. S1A**), for which all lines and clones showed similar positive expression. The differentiation of iPSCs to ECs–through mesoderm and subsequently endothelial specification (5) (**Fig. S1B**)–resulted in endothelial populations of 95+% purity via vascular endothelial cadherin (VE-Cadherin) expression across single non-risk, risk wildtype, and risk knockout lines (**Fig. S1C**) when assessed by flow cytometry. Moreover, staining for junctional proteins ZO1 and VE-

Cadherin showed appropriate localization (**Fig. 1A**) and no noticeable morphological differences in circularity independent of the haplotype (**Fig. S2**). To ensure that basic EC lipid uptake was not affected by haplotype, iPSC-ECs were assessed for acetylated-LDL uptake, and we found that population percentage uptake was not impacted by the presence or absence of the polymorphisms (**Fig. S1D**).

Morphological and functional assessments suggest that maturity is haplotype independent, but to ensure that this extends to the transcriptional level, we performed RNA-sequencing on iPSC-ECs, specifically of R/R WT and KO lines from two patients (C512 and C021), i.e. two clones from one patient (R/R WT clones 1-5 and 2-3 and isogenic R/R KO clones 1-9 and WB46) and one from the second patient (R/R WT clone ED2-70 and R/R KO clone ED2-65), and two differentiation batches of one isogenic clone pair (e.g., 1-5 and 1-9). A Pearson correlation plot of the entire transcriptome showed greatest clustering by patient and then by clone, with consistent clustering of haplotype pairs with multiple differentiations under static conditions (**Fig. 1B**); indeed, 3D principal component analysis (PCA) of the transcriptome groups by haplotype revealed little overall sorting (**Fig. 1C**). Closer inspection of transcriptional differences indicated only 13 genes were differentially expressed genes (DEGs) for WT versus KO, i.e., those with an adjusted p-value threshold of 0.1 and expression difference of >2-fold. However, when including genes with statistically different expression regardless of magnitude (86 total), we observed small fold-changes under static conditions (**Fig. 1D-E; Supplemental Table 1**). Consistent with these observations, the most significant 20 gene ontology (GO) terms via Fisher's exact test included broad cardiovascular response

categories (**Fig. 1F**, red; **Supplemental Table 2**); those terms related to blood flow and forces (open arrowheads) and to inflammation (closed arrowheads) are highlighted, and suggest that they are possible signaling mechanisms.

Figure 2.1. 9p21 CAD risk haplotype does not impact EC commitment but does prescribe some transcriptome differences (A) Images of nuclei (DAPI; blue), VE-cadherin (yellow), and ZO1 (green) for cells of the indicated haplotypes. Arrowheads indicate positive staining of proteins at the cell-cell junctions. Scale bar is 10 microns. (B) Pearson's Correlation plot is shown for patient iPSC-derived ECs based on the whole transcriptome sequenced from the patients, clones, and haplotypes indicated at right. Dendrogram indicates sample clustering; the color map is plotted between 0 and 1 as consistent with other figures. (C) Independent of patient and clonality, a 3D PCA plot is shown for transcriptomes from R/R WT (red) and R/R KO (yellow) ECs. Individual samples are shown as smaller spheres whereas sample averages are indicated by a larger sphere noting its linkage via identically colored lines. The contribution of each PCA axis is noted alongside the axis itself. (D) Volcano plot and (E) heatmap of 111 DEGs for transcriptomic comparisons of R/R WT (red) and R/R KO (yellow) ECs. Colors indicate in which haplotype were the genes upregulated. Color map also indicates the strength of expression in terms of Fragments Per Kilobase of transcript per Million (FPKM) mapped reads. (F) Top 20 gene ontological terms are plotted with their statistical significance and colored based on their association to cardiovascular stress; open and closed arrowheads correspond to ontologies related to blood flow and forces and to inflammation, respectively.

Figure 1 **Teng et al**

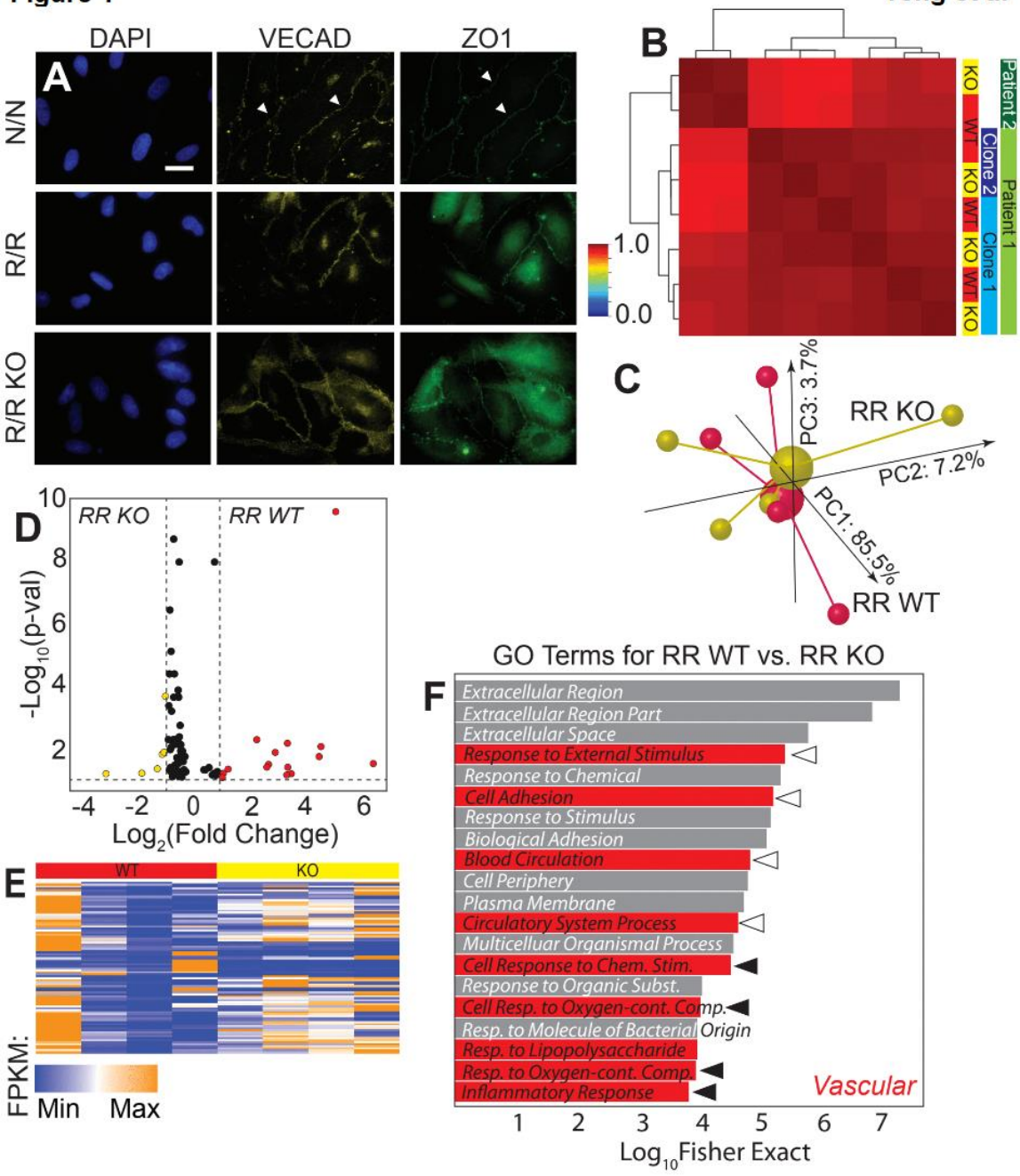

2.3.2 Inflammatory signaling impairs iPSC-EC function but not transcription based on haplotype

The presence of inflammation GO terms and prior implication of inflammation in 9p21 pathogenesis (67) led us to first assess the role that inflammatory cytokines, e.g., TNFα, could have on iPSC-EC haplotype-dependent function. iPSC-ECs cultured in 2D on transwell inserts were challenged after monolayer formation by exposure to TNFα, and apparent permeability was assessed. We found that risk cells were the most permeable with highest transmission of a 70 kD fluorescent dextran between chambers; removal of the locus partially restored barrier function (**Fig. 2A**; red vs. yellow). Treatment with TNFα for 12 hours increased permeability independent of haplotype, but cells containing the risk haplotype remained most permeable with removal of the locus partially restoring function relative to non-risk cells (**Fig. 2A**; +TNFα). GO terms for untreated cells were suggestive of a mechanism involving ROS secretion, and immunofluorescent assessment indicated reduced signaling when the locus was deleted (**Fig. 2B**). These data suggested that the haplotype could be mediating transcriptional regulation induced by stress, e.g., inflammation, as we previously observed in other cell types with stress (71, 72).

To further understand the extent that TNFα caused haplotype-dependent transcriptional changes, we performed RNAseq on TNFα-treated iPSC-ECs. While the transcriptomes of unstimulated cells were sorted based on patient, clone, and then haplotype, a Pearson correlation plot of all transcripts from TNFα-treated cells indicated only subtle variation (**Fig. 2C**), consistent with functional observations, and not by patient or clone as with untreated cells in Figure 1. While 2D PCA does indicate modest

haplotype clustering (**Fig. 2D**), TNFα treatment resulted in fewer DEGs when comparing WT to KO cells (**Fig. 2E**, red) to the same comparison with untreated cells; there were no statistically significant GO terms with this dataset. The lack of transcriptional changes with TNFα treatment while simultaneously having observed permeability changes suggested that regulation by the haplotype might not be transcriptional, unlike what we previously observed in other cell types when stressed (71, 72). Since prior studies examined mechanical stresses, we next sought to understand how and to what extent iPSC-ECs respond in a more physiologically relevant niche to fluidic stress.

Figure 2.2. Inflammatory cytokine impact on EC barrier function depends on risk haplotype
(A) Apparent permeability is plotted as a function of risk haplotype and the presence or absence of TNFα. ****$p < 0.0001$ for indicated comparisons via one way ANOVA with multiple comparisons Tukey test. n = 18-24. **(B)** Representative immunofluorescence images stained for ROS for the indicated risk haplotypes. At right, average cell intensity is quantified for n = 16-17 cell fields of view over triplicate experiments for R/R WT and KO, respectively. **$p < 0.01$ for indicated comparisons via unpaired t-test. **(C)** Pearson's Correlation plot is shown based on the whole transcriptome sequenced from patient iPSC-derived ECs treated with TNF and of the haplotypes indicated at right. Dendrogram indicates sample clustering; color map is plotted between 0 and 1 as consistent with other figures. **(D)** A 2D PCA plot is shown for transcriptomes from R/R WT (red) and R/R KO (yellow) ECs; patient origin is noted by an outline around each data point. The contribution of each PCA axis is noted alongside the axis itself. **(E)** Mean transcript expression is plotted as a function of the log ratio of change between WT and KO for all transcripts. Data in red represent genes with statistically significant differential expression based on DESeq2.

Figure 2 **Teng et al**

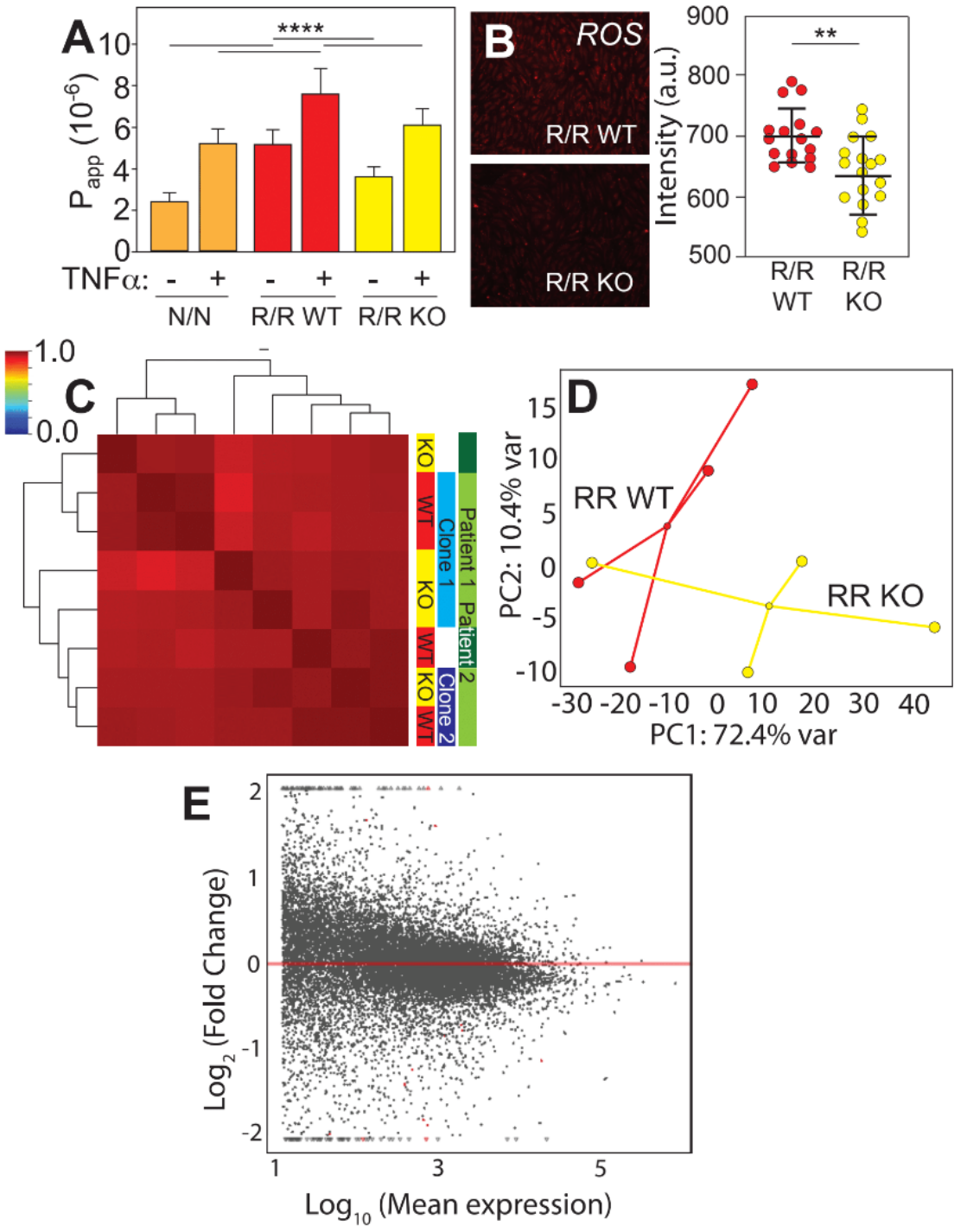

2.3.3 Acute shear stress impairs iPSC-EC function via haplotype-based transcriptome regulation

Endothelial cells are constantly exposed to shear stress *in vivo*. Under these conditions, the increased susceptibility to CAD due to 9p21 risk SNPs *in vivo* (81-83) and subsequent mechanisms may be more pronounced in iPSC-ECs when exposed to shear stress. Thus, we constructed a microfluidic device consisting of a single-channel 3D microvessel (**Fig. S3**), which exposes cells to laminar shear stress based on Poiseuille flow (84). iPSC-ECs were seeded within the media-filled collagen scaffold and allowed to form a monolayer within the microvessel channel under <1 dynes/cm2 fluid flow (**Fig. 3A, A'**; **Fig. S4A-C**); this simple design enabled us to perfuse vessels with 70 kD fluorescent dextran and measure apparent permeability in 3D via radial diffusion through the microvessel monolayer outwards to the lumen (**Fig. S4D**). For iPSC-ECs derived from R/R WT and R/R KO lines, we measured permeabilities when exposed to a range from 1, 30, 60, or 100 dynes/cm^2 for 24 hours. Overall, both risk haplotype and shear stress were statistically significant variables by two-way ANOVA ($p<0.0001$). More specifically, at physiological shear (<30 dynes/cm^2) (85-87), apparent permeability was significantly increased for the risk haplotype compared to their KO isogenic counterpart microvessels. However, permeability was insensitive to changes in shear in this range (**Fig. 3B**). On the other hand, above 30 dynes/cm^2, apparent permeability increased more at intermediate shear for R/R WT than their isogenic counterpart R/R KO cells (**Fig. 3B'**); in this pathological shear range for CAD (87), monolayer integrity was lost (**Fig. S5**). Much above this range at 100 dynes/cm^2, apparent permeability differences were lost ($p=0.99$) as was monolayer integrity for both haplotypes. These data suggest that the

microvessels of risk haplotype are more susceptible to vessel dysfunction at pathological shear but that deletion of the haplotype rescues the phenotype.

To determine the transcriptional changes associated with the onset of risk haplotype dysfunction, we performed RNA-sequencing on iPSC-ECs exposed to 30 dynes/cm^2 which is the point of pathological shear onset for CAD (87), where we observed significant differences in permeability despite having an intact monolayer (avoiding selection bias). A Pearson correlation plot of the entire transcriptome under acute shear showed stronger clustering by patient and clone than haplotype (**Fig. 3C**) versus static conditions. However when clustering by haplotype alone in a 3D PCA plot and unlike with static conditions, we still observed substantial separation based on the entire transcriptome (**Fig. 3D**). These data suggest that shear stress actives haplotype regulation on the transcriptome. What could result from such regulation is an increase in the number of DEGs between WT and KO cells; thus, we also examined DEGs under shear, defined here as an adjusted p-value of 0.1 and expression difference of >2-fold. With these cutoffs, we detected 135 DEGs between WT and KO cells as a result of shear (**Supplemental Table 3**). The number of DEGs when cultured with shear is nearly 10-fold higher (**Fig. 3E**) than without.

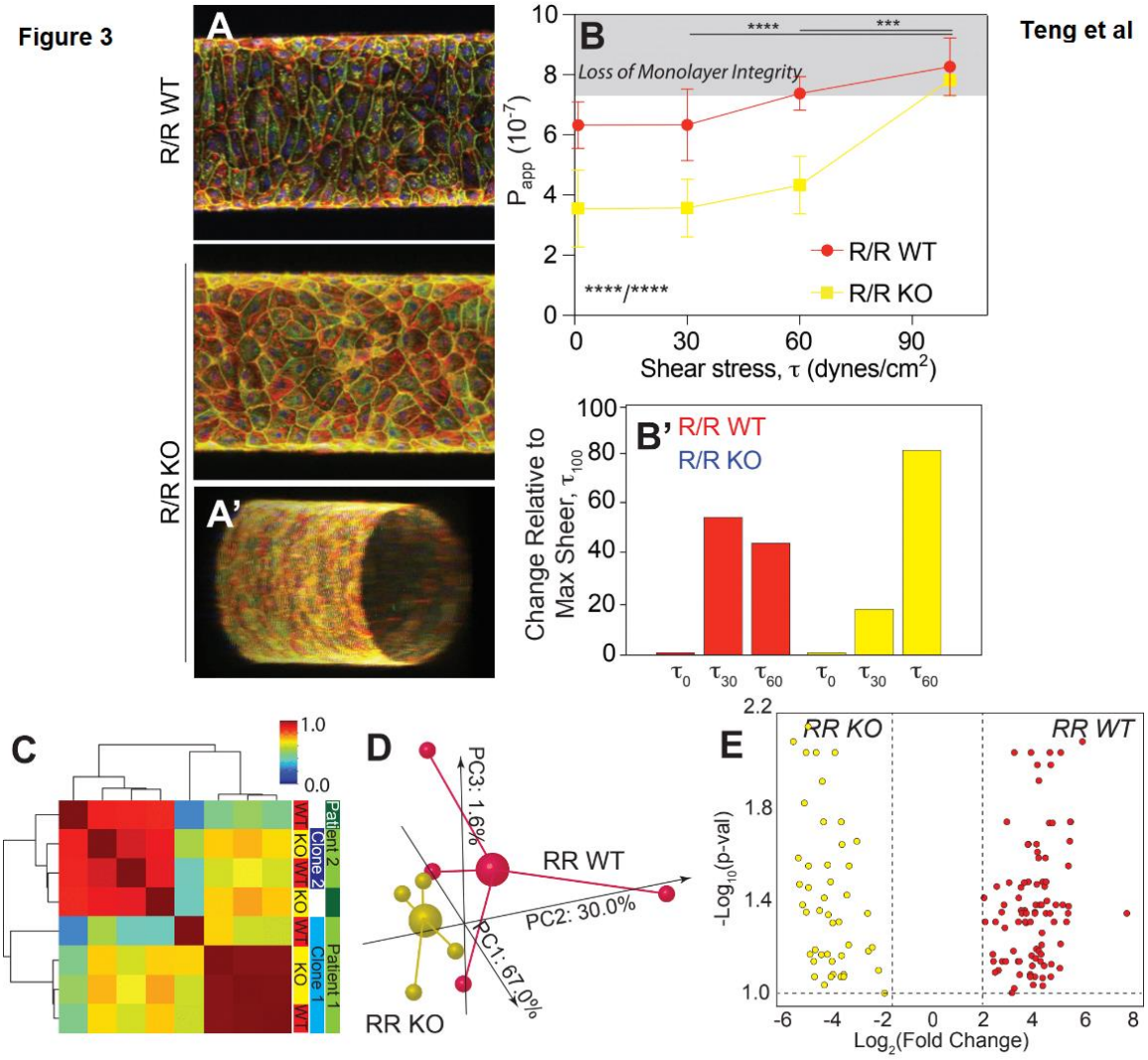

Figure 2.3. Exposure to acute shear reduces EC barrier function for the risk haplotype
(A) Representative images of iPSC-ECs cultured in cylindrical vessels for 7 days and stained for ZO1 (green), F-actin (red), VE-cadherin (yellow), and nuclei (blue). R/R WT (top) and R/R KO (bottom) are shown, with the latter including an oblique view to illustrate patency. (B) Apparent permeability, measured by dye exclusion assay, for R/R WT (red) and R/R KO (yellow) increases with acute exposure to shear. ****$p < 0.0001$ for shear and haplotype based on one way ANOVA with multiple comparisons Tukey test; ***$p<0.001$ and ****$p<0.0001$ for shear and haplotype comparison based on two-way ANOVA with multiple comparisons Tukey test. Note that in panel B', the percent change in slope relative to maximum acute shear is plotted (i.e., the percent difference in the average values), highlighting the early onset of monolayer integrity loss as noted in Supplemental Figure 5. n = 3-6 per haplotype and shear stress. (C) Pearson's Correlation plot is shown for patient iPSC-derived ECs based on the whole transcriptome sequenced of the haplotypes indicated at right. Dendrogram indicates sample clustering; color map is plotted between 0 and 1 as consistent with other figures. (D) Independent of patient and clonality, a 3D PCA plot is shown for all transcriptomes from R/R WT (red) and R/R KO (yellow) ECs cultured in the vessel geometry for 6 days followed by acute shear stress for 24 hours. Individual samples are shown as smaller spheres whereas sample averages are indicated by a larger sphere noting its linkage via identically colored lines. The contribution of each PCA axis is noted alongside the axis itself. (E) Volcano plot of 203 DEGs for transcriptomic comparisons of R/R WT (red) and R/R KO (yellow) ECs identified by DeSeq2 with an adjusted p-value threshold of 0.1. Colors indicate in which haplotype were the genes upregulated.

To investigate potential shear-mediated haplotype-specific mechanism, we next plotted the most significant gene ontological terms by Fisher's exact test, finding that of the top terms, those associated with extracellular matrix (ECM) and cell adhesion were most abundant (**Fig. 4A; Supplemental Table 4**), suggesting that loss of monolayer integrity at even higher shear could be a result of haplotype-specific transcriptional silencing of cell adhesion receptors. To further confirm the effects of shear on adhesion and ECM and eliminate underlying variance from the haplotype alone, we compared transcriptome differences between isogenic WT and KO pairs in shear and static conditions. As shown in **Fig. 4B**, overall variance was greater with shear, hence the elongated distribution. Genes differentially expressed in the sheared WT/KO ratio (red) tended to show larger and more numerous effects than in static conditions (blue). This was especially pronounced for transcripts associated with adhesion and ECM (green outlined data); genes within these ontologies largely changed from down- to up-regulated with shear, perhaps to counteract haplotype effects resulting in monolayer loss. However, to interpret these data in a network context, we next mapped isogenic WT and KO pairs in shear versus static conditions onto common CAD pathways present in Ingenuity Pathway Analysis (IPA). A diagram of signaling connections (**Fig. 4C**) illustrate potential haplotype signals; pathways that positively regulate cell adhesion appear to increase with shear in KO cells (green), whereas those that negatively regulate cell adhesion appear increased in WT cells (pink). Therefore, we performed a comparison of these data to known CAD genes identified from meta-analyses, e.g., the CARDIoGRAMplusC4D consortium (88) as well as others (89, 90). From these studies,

91 genes associated with 88 loci are suggested to be dysregulated in CAD. Genes differentially expressed in the presence of the risk haplotype, that appeared to be shear-sensitive, and that overlap with CAD-associated genes were found on multiple chromosomes indicating wide haplotype regulation; in general, weakly upregulated genes in static conditions for R/R KO reversed and became more strongly upregulated in R/R WT under shear (**Fig. 4D; Supplemental Table 5**). In addition to global CAD risk activation upon exposure to pathologically high shear, several CAD-associated genes were found in both static and shear conditions with opposing expression. TNS1 and CAMSAP2 (**Fig. 4D**; red), for example, relate to cellular mechanical functions such as cytoskeletal stability, which aligns with previous ontologies and IPA. Overall, these data suggest that mechanical regulation of endothelial cell function could be haplotype-specific and modulated by high shear stress.

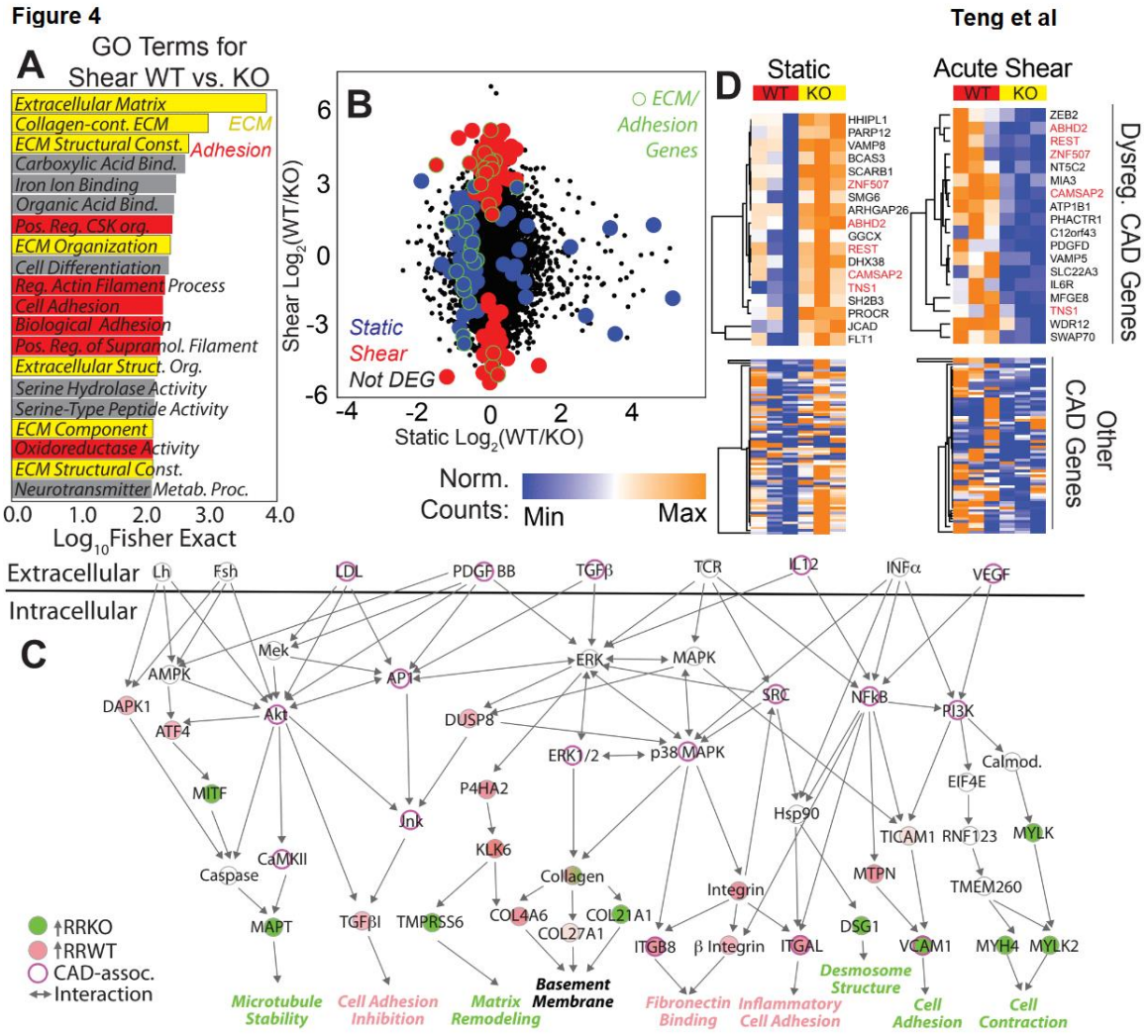

Figure 2.4. Shear mediated haplotype regulation affects adhesion and CAD transcriptional signatures
(A) Top 20 statistically significant GO terms for the R/R WT vs. KO comparison from the TopGO library. Terms associated with ECM (yellow) and adhesion (red) are indicated. (G) Scatter plot is shown of the $\log_2$ fold change of the R/R WT to KO ratio for each transcript of iPSC-ECs from sheared and static conditions. Black data points indicate non-DEGs, blue indicates DEGs for static only, and red indicates DEGs for shear only. Data points outlined in green represent those associated with ECM or adhesion GO terms. (C) Ingenuity analysis identified several differentially expressed genes in signaling pathways linked to CAD via the IPA database. Coloring of gene nodes indicates upregulated expression relative to R/R WT (red) or R/R KO (green). CAD associated genes via IPA database and previous literature are shown with purple highlighted outline. (D) Heatmaps showing gene expression for non-zero genes whose loci have been linked to CAD via the CARDIoGRAMplusC4D study. Values shown were computed by DESeq2's median of ratios. Top heatmaps show statistically significant CAD associated genes between R/R WT (red) and KO haplotypes (yellow). Bottom heatmaps show expression of the other genes identified from the CARDIoGRAMplusC4D study (bottom). Genes sorted into the top heatmaps had $p<0.1$ for unpaired t-tests. Left and right heatmap columns are for iPSC-ECs under static or acutely sheared conditions, respectively. DEG names are shown to the right of top heatmaps with red highlighting indicating common genes between conditions.

2.4 Discussion

While correlations found with genome wide-association studies have identified many SNPs related to disease (65, 66), mechanisms for those in non-coding loci are not well understood, e.g., the non-coding 9p21 locus and risk of endothelial permeability and disease. Difficulties could result from the linkage disequilibrium of the locus' polymorphisms (67), multiple, overlapping disease risk factors (91), contradictory behavior of animal models (41, 92), or the requirement of a covariant stressor (71, 72). Here we found that iPSC-derived endothelial monolayers had increased apparent permeability under static conditions with the risk haplotype and when stressed with an inflammatory cytokine. More strikingly, when placed in a microvessel under high, acute shear stress consistent with CAD (85-87), endothelial cells with the risk haplotype exhibited increased apparent permeability compared to KO cell types in part because of the loss of monolayer integrity, similar to the leaky vasculature observed clinically with CAD (93). Only at supra-pathological shear stress (87), e.g., 100 dynes/cm^2, did KO cell monolayer lose integrity and approach the same permeability as their risk WT counterparts. Detailed analyses of known CAD genes (88-90) and pathways further implicate adhesion changes as a potential mechanism for haplotype-mediated changes. These results suggest that mechanical stress pathway(s) can induce EC dysfunction more than inflammatory cytokine TNFα and that shear stress causes dysfunction in a haplotype-dependent manner via modulating cell-cell and cell-ECM adhesion gene expression. Alongside our prior work (72), these data are generally supportive of the framework where environmental interactions act in concert with genetic variants to induce iPSC-derived progeny responses similar to in vivo assays, which may be impractical or impossible in common laboratory animals (41, 42, 69).

The effects from both excessive wall shear stress and inflammation are well known in CAD, e.g., EC barrier function is highly susceptible to inflammatory cues (77). For the 9p21 locus, cytokines such as TNFα and IL-6 are higher in patients with the risk haplotype (94). Interferon signaling is also a known regulator of this locus' activity (67), which implies that in the presence of the risk haplotype, CAD progression might also occur indirectly via transcriptional regulation. Conversely, CAD risk factors also include the presence of turbulent flow or high magnitude oscillatory flow (80), both of which can damage the endothelium (79). Until this study, however, it was unclear if high wall shear stress could regulate the activity of a non-coding locus in and of itself and similarly influence cell function. Here we found that not only was the TNFα effect marginal on iPSC-derived ECs, it was insensitive to the risk haplotype; only minor differential transcriptional regulation was detected as a function of haplotype. However, significant functional and transcriptional changes occurred when cells were perfused slowly in a microvessel model for an extended period and then exposed to acute, high wall shear stress. The implication from these data is that transcription changes with shear mirror some gene activation patterns found in the meta-analyses of CAD transcriptional differences (88-90).

High shear flow resulted in increased EC permeability and diminished monolayer integrity, which are clinical hallmarks of disease (87, 95). At shear stresses just prior to EC detachment, we found a switch from down- to up-regulation of a subset of cell adhesion genes, perhaps to counteract haplotype-specific loss of cell-cell regulators, e.g., risk WT cells exhibited a 25-fold reduction in VCAM. Indeed, both IPA and GO analyses

showed knockout cells expressing pathways related to contractility, cell-cell adhesion, and ECM; conversely, the risk haplotype expressed inhibitory pathways. Although a 9p21-specific relationship with shear and adhesion has not been previously documented, stress-mediated monolayer disruption in ECs has been noted both in vitro and in vivo (71, 76, 79) and suggests some fidelity between model observations and clinical presentation. In parallel, cytokines are classically known to activate endothelial cell expression of leukocytes adhesion receptors (96), which facilitates their migration into subintimal spaces. We observed similar changes in risk WT ECs, albeit when exposed to acute shear stress. Leukocyte infiltration can be extremely detrimental to established disease (95, 96), hence concern from a 13-fold upregulation of Integrin α_L with risk haplotype. When present, leukocyte signals (97) have even mirrored the cell erosion observed here at high shear stress. Thus, adhesion modulation appears in multiple mechanisms of CAD, and 9p21 could play a part in that mechanism.

Finally, the combination of iPSC-derived ECs and a 3D microvessel model afforded us a unique opportunity to study disease in a more appropriate setting *in vitro*; as previously noted, particular loci are found only in evolutionary relatives of humans and not in common laboratory species (42, 69), complicating disease models. Patient-derived iPSCs have been used as an alternative (70), but standard culture conditions may not induce the regulation one intends to study owing to a locus' variable penetrance or its indirect effects on disease (98). Conversely, significant effort over the past two decades has resulted in a wide variety of biomaterials and fabrication methods to create the appropriate context in which to test a hypothesis about genetic regulation of disease. Our own recent evidence suggests that microenvironmental changes are necessary, e.g.,

stiffening of the niche (72), to induce expression of lncRNA in the risk haplotype. Only at that point does their presence cause asynchronous contraction of iPSC-derived cardiomyocytes. Similar time-dependent stiffness changes can induce subtle but more physiologically appropriate initiation of epithelial-to-mesenchymal transition (99, 100) or loss of progenitor cell potency (101). The microfluidic vessel used in this study similarly induced haplotype regulation upon exposure to acute, high shear stress. However, CAD flow patterns are exceedingly complex (87, 95), and further refinement of our model, e.g., inclusion of baffles to create turbulence, could better refine our system further and perhaps uncover additional regulation of the niche on the risk haplotype.

2.5 Methods

2.5.1 Ethical compliance and cell lines

The authors have complied with all ethical regulations. Human subjects were enrolled and informed consent obtained under a study approved by the Scripps IRB (11-5676) and cells were transferred and maintained under a study approved by UCSD IRB (#141315). The lines included in this study were from three patients: C151 (N/N; clone WF9), C512 (R/R WT clones 1-5 and 2-3 and isogenic R/R KO clones 1-9 and WB46), and C021 (R/R WT clone ED2-70 and isogenic R/R KO clone ED2-65). Isogenic KO lines were derived by TALEN-mediated genome editing as previously described (71)

2.5.2 Endothelial cell (EC) differentiation

iPSCs were differentiated into ECs using an established protocol (5) (**Fig. S1B**). Briefly, iPSCs were plated at densities ranging from 32,000 to 52,000 cells/cm^2 on Day 0.

Cell media was then changed to N2B27 + CHIR media on Day1. Cell media was changed to Stempro + Forskolin + VEGF on Day4. Cell media was again changed on Day5. Cells were sorted on Day 6 using Flow Assisted Cell Sorting (FACS) for VE-Cadherin immunostaining and plated for 7 days for endothelial maturity.

2.5.3 Immunofluorescence imaging

Cells were immersed in an ionic solution of 1 mM MgCl2 and 0.1% (w/v) Saponin for the duration of the immunostaining. Between each step, the sample was washed three times with 1mM MgCl2 solution. Cells were introduced to only 0.1% (w/v) Saponin for 15 minutes before blocking with 2%Goat Serum solution for 30 minutes. Primary antibody solution was added into saponin and goat serum solution as noted before added to the sample for 2 hours. These antibody solutions include VE-Cadherin 1:100 concentration (Cell Signaling D8752) and ZO1 1:200 (Abcam 221546). Secondary fluorescent antibodies were added 1:1000 to the samples in the goat serum + saponin solution for 45 minutes at room temperature. Additionally, rhodamine phalloidin may be added for actin visualization. DAPI dye was then added to the sample for 3 minutes at a 1:400 dilution. The sample was then prepared using fluoromount on a microscope slide for imaging (**Fig. 1A**). Cells were imaged using Zeiss 780 Confocal Microscope.

2.5.4 Circularity Analysis

Immunofluorescent stained endothelial cells were stained using immunofluorescent staining techniques and ZO1 antibody as described earlier. Samples were imaged using Zeiss 780 confocal Microscope. Cell area and perimeter were

measured using ImageJ software. Circularity was calculated using the cell area and perimeter measured (**Fig. 1B**).

2.5.5 ROS detection assay

Mature and confluent endothelial monolayers were washed twice with PBS before being immersed in a 5 μM dihydroethidium solution at 37^{o}C for 20 minutes. Samples were then washed twice with 1mM $MgCl_2$ solution before being fixed using 10% formaldehyde solution. Samples were then mounted and imaged as described above (**Fig. 2C**). Cell nuclei intensity were then measured using ImageJ software.

2.5.6 Dye exclusion assay

iPSC-derived endothelial cells were cultured on a transwell permeable support for 6 days. On the sixth day, cells were serum starved for 24 hours before the start of the assay. In some sample groups, TNFα was added to the solution at 1ng/mL in serum starve conditions 12 hours before assaying. A 24-well plate fitting the corresponding permeable transport was filled with 600 μL media solution for each well for each time point and permeable support. The top compartments of each permeable support were replaced with new media at the start of the assay also containing 0.2 mg/mL 70kDa FITC-Dextran at the start of the assay. Over a period of one hour at 15-minute intervals, the permeable support containing confluent endothelial cells was transferred from one well to a new well. Samples of each time point and each permeable support were then transferred to a 96 well plate for imaging in a Syngery 4 multi-mode microplate reader (**Fig. 2A**). Using a FITC-Dextran standard, mass diffused over time and apparent permeability were calculated.

2.5.7 RNA isolation

Cells were lysed with Trizol. Chloroform was added 1:5 to trizol and moved to Eppendorf microcentrifuge tubes. Samples were then spun down at 14,000rpm for 15 minutes using an Eppendorf Centrifuge 5424 R. Aqueous solution separated during centrifugation was removed from the top of samples and mixed 1:1 with Isopropanol and made to sit for 10 minutes at 4^{o}C before centrifugation at 14,000rpm for 10 minutes. The sample supernatant was then removed and replaced with 75% ethanol with DEPC water before centrifugation at 11,000rpm for 5 minutes. The supernatant was once again removed and the sample-containing Eppendorf tubes allowed to dry for 10 minutes. Sample pellets were then resuspended in DEPC water and the RNA concentration calculated using a Thermofisher Nanodrop 2000C. In the event of having small cell quantities to work with, a Qiagen miRNeasy kit was used for RNA extraction. The kit protocol was followed as instructed.

2.5.8 Quantitative PCR

Cell-isolated RNA was made into cDNA for quantitative PCR analysis using the Invitrogen Superscript III reverse transcriptase kit. cDNA was aliquoted into a 384-well plate according to the number of primers being used and a mixture of primers, DEPC water, and Power SYBR Green PCR master mix was added to each sample aliquot. This 384-well plate was then read in the BioRad CFX 384 Touch Real-time PCR Detection System.

2.5.9 Creation of microvessel model

Glass-bottom petri dishes were used as the frame of the devices in a process outlined in **Fig S3.** Holes of 0.64 mm and 1.27 mm were drilled into opposite sides of the petri dishes, directly above the bottom of the petri dish and perpendicular to the petri-dish wall. Blunt-end pins of 23 G and 18 G (0.25 in)' were fit snugly into the drilled holes, making sure to not allow for unusual cracks or holes. A steel cylinder was then fit from one end of the petri dish to the other through the blunt end pins. PDMS with ratio of crosslinker 1:10 elastomer was then poured to fill the modified dish and allowed to solidify. PDMS was degassed prior to addition to the mold to ensure smooth interface. After the PDMS had solidified, the chamber dimensions were created by removing PDMS from the modified dish. The blunt-end pins were allowed to extend beyond the wall of the chambers to disperse pressure away from the collagen-PDMS interface and instead further into the collagen gel and the lumen. The gel chamber is cleaned to remove any small PDMS residue. The seal of the bottom glass and the petri-dish were ensured intact and unbroken. Freshly made PDMS is then poured into a petri-dish lid according to the volume of the intended gel chamber, being sure to not create bubbles. The modified dish is then inverted and placed over the fresh PDMS in the lid to seal the gel chamber. The PDMS was not allowed to rise to the blunt-end pin openings of the gel chamber in order to allow for unobstructed inlet and outlets of the gel chamber. The modified dish is then allowed to rest for at least two days.

To create the gel scaffold within the microfluidic devices, all components, including the PDMS-dish case, the blunt-end pins, and any other framework supports, such as the microfluidic stand, were sterilized. The blunt-end pins were then fit into the appropriately sized holes in the PDMS-dish case. Any introduction of liquid to the device

was then added via leur-lock syringe through the inlet only, which has a smaller diameter than the outlet, to minimize pressures within the gel chamber. The chamber is washed once with PBS, then coated with 0.1mg/mL Poly-D-lysine for 5 minutes before being washed out with PBS. This is set to dry overnight.

Type 1 collagen gel was used for the gel scaffolding for all experimentations within the microfluidic device. For a 6 mg/mL concentration collagen gel, 1 M NaOH at 0.024 the volume of collagen and 10x PBS at 0.1 the total volume were mixed together in a small petri dish on ice. Type 1 collagen gel, chilled on ice, was mixed well into the NaOH and PBS mixture until uniformity, avoiding bubble formations. Deionized water was added and mixed to fill the remaining total volume. The finished type 1 collagen gel mixture was then syringed into the microfluidic device from the inlet slowly, allowing for minimal bubble formation but before warming of the gel occurs, until the entire gel chamber is filled and half way into the outlet blunt-endpin. A thin steel cylinder of 340 μm diameter was then inserted through the inlet, and the outlet was then gently sealed with a male leurlock plug. The device was then heated at 37^{o}C in an incubator with the outlet side up for 2 hours for gel solidification. 2 hours after solidifying, the microfluidic device was removed from the incubator and the thin steel cylinder was removed gently from the device. The channel was then inspected for any obstructions and flow tested from outlet to inlet. The collagen gel is then crosslinked with a 20 mM genipin solution for 2 hours at 37^{o}C. After 2 hours, the microfluidic device was washed with PBS at room temperature. The device was washed with PBS overnight at room temperature to remove any residual genipin solution.

2.5.10 Preparation and use of microvessel model

After overnight PBS wash, the microfluidic devices were coated along the lumen of the collagen scaffold with 0.1 µg/mL fibronectin for greater cell attachment during seeding (**Fig S4B)**. Each side was coated for an hour with fibronectin solution for even distribution on all sides of the microfluidic channel. With coating complete, the microfluidic device was perfused overnight with EGM2 media at room temperature to allow for displacement of PBS-scaffold liquid for cell nourishing media.

To seed cells into the microfluidic device, a device was placed at 37^{o}C in an incubator 30 minutes before seeding to warm up the media and device. Endothelial cells were lifted and prepared in solution at 10 million cells/mL in EGM2. 8 µL of cell solution was then pipetted into the device through the inlet, allowing for the cell solution to flow through and into the lumen of the device, and then the microfluidic device was placed in the incubator for 5 minutes. After incubation, the device was reseeded with another 8 µL of cell solution again and placed on another side of the device for 5 minutes in the incubator, and continuing for the other side and top of the device. This allowed for even distribution of cells along all sides of the device. After seeding all four sides of the device (top, sides, bottom), the microfluidic device was placed in the 37^{o}C incubator to allow for cells to strengthen attachment. One hour later, fresh media was added to the microfluidic device. 10 hours later, the microfluidic devices were connected to a peristaltic pump for long term perfusion. Media reservoirs were changed with fresh media every 2 days.

2.5.11 Microvessel permeability assay

On the sixth day of pump perfusion, the microfluidic shear is increased to the desired shear stress magnitude and held for 24 hours. After perfusion, microfluidic

devices were gently removed from the pump perfusion and attached to a microscope slide. The microfluidic device was then mounted on the microscope platform of a Zeiss 780 confocal microscope. The image area was centered on the channel to allow for observation of diffusion. The microfluidic device was then perfused at approximately 0.4 µL per minute with 0.2 mg/mL 70kDa FITC-Dextran dye in EGM2 media over 30 minutes, with fluorescent images taken every 2-minutes (**Fig. S4D**). The fluorescent intensity of a consistently standardized area around the microfluidic channel is then measured for each image using ImageJ software. Change in fluorescence intensity is calculated over time, which is then used to calculate apparent permeability of the microfluidic device based on channel dimensions.

2.5.12 RNA sequencing

Isolation of RNA was conducted as described above. Samples were submitted to UCSD Institute for Genomic Medicine Sequencing Core. Total RNA was assessed for quality using an Agilent Tapestation 4200, and samples with an RNA Integrity Number (RIN) greater than 8.0 were used to generate RNA sequencing libraries using the TruSeq Stranded mRNA Sample Prep Kit with TruSeq Unique Dual Indexes (Illumina, San Diego, CA). Samples were processed following manufacturer's instructions, modifying RNA shear time to five minutes. Resulting libraries were multiplexed and sequenced with 100 basepair (bp) paired end reads (PE100) to a depth of approximately 25 million reads per sample on an Illumina NovaSeq 6000. Samples were demultiplexed using bcl2fastq v2.20 Conversion Software (Illumina, San Diego, CA). Analysis was conducted using STAR, R, DeSeq2, and python software.

2.5.13 Statistics

All experiments were performed using cells from three distinct differentiations with the number of technical replicates, n, indicated where appropriate. Bar graphs and scatter plots with individual data are represented as mean ± standard deviation. Statistical analyses were performed using GraphPad Prism5, the threshold for significance level at $p<0.05$ unless otherwise noted, and are detailed in the corresponding figure legends.

2.5.14 Data and software availability

The accession number for the RNA-seq data reported in this paper is GEO: 21738935. The authors declare that all data supporting the findings of this study are available within the paper and its Supplementary Information. Source data for the figures are available from the corresponding author on reasonable request.

2.6 Supplementary Figures

Supplementary Figure 2.1. Endothelial differentiation occurs independent of risk haplotype
(A) Representative images of iPSC derived from patients for the indicated genotype at 9p21, i.e., non-risk (N/N), risk (R/R), and isogenic lines where the risk haplotype was knockout via TALEN (R/R KO). Images show nuclei (DAPI; blue), Sox2 (green), Nanog (red), and Oct4 (white). Scale bar is 100 microns. **(B)** Timeline with corresponding media and growth factor conditions as well as phase contrast images of cells. Relative developmental stage or lineage is shown at bottom. Scale bar is 100 microns. **(C)** Flow cytometry plot of vascular endothelial cadherin (VE-Cadherin) from non-risk and risk wildtype lines. Gates were created based on staining from positive and negative control expression with human umbilical vein endothelial cells (HUVECs). **(D)** Uptake of acetylated-LDL was observed by fluorescence (representative image) and assessed by flow cytometry for all haplotypes; N/N and R/R WT are shown as representative plots. Gates were created based on acetylated-LDL staining from HUVECs. Scale bar is 50 microns.

Supplemental Figure 1 **Teng et al**

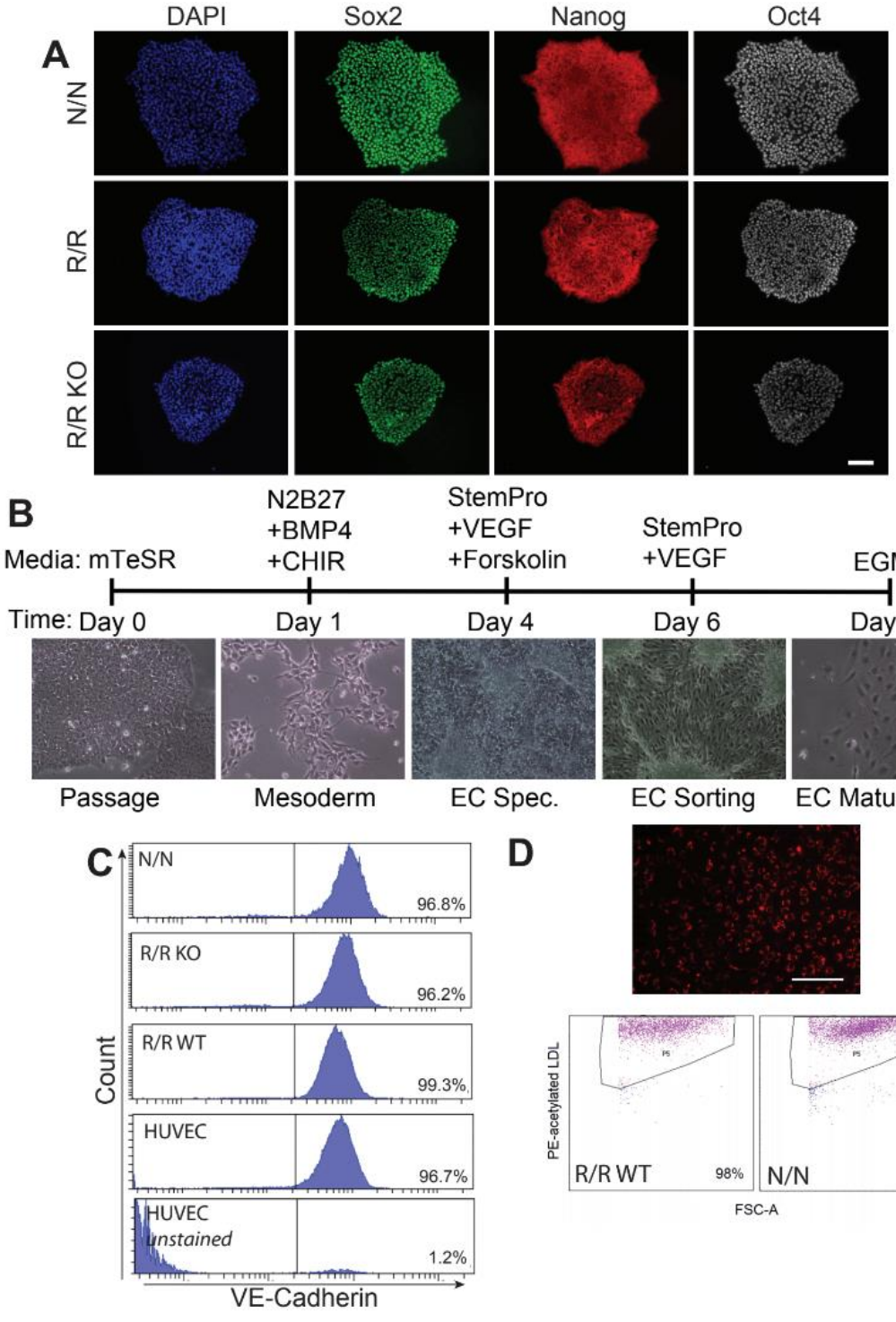

Supplemental Figure 2 **Teng et al**

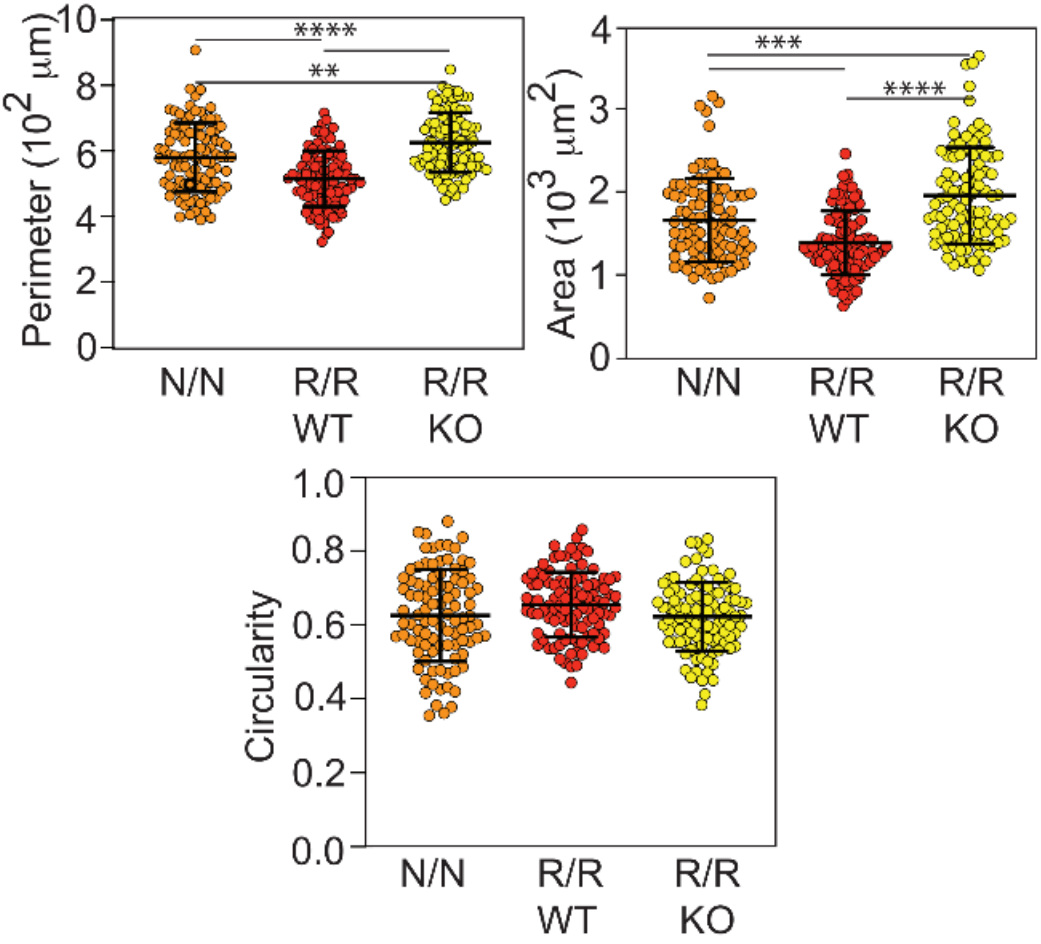

Supplementary Figure 2.2. Endothelial morphology differences as a function of risk haplotype
Plots of cell morphology for cells of the N/N (orange), R/R WT (red), and R/R KO (yellow) haplotypes showing cell area, perimeter, and circularity. Averages and standard deviations are noted in black. No statistical differences were observed in cell circularity.

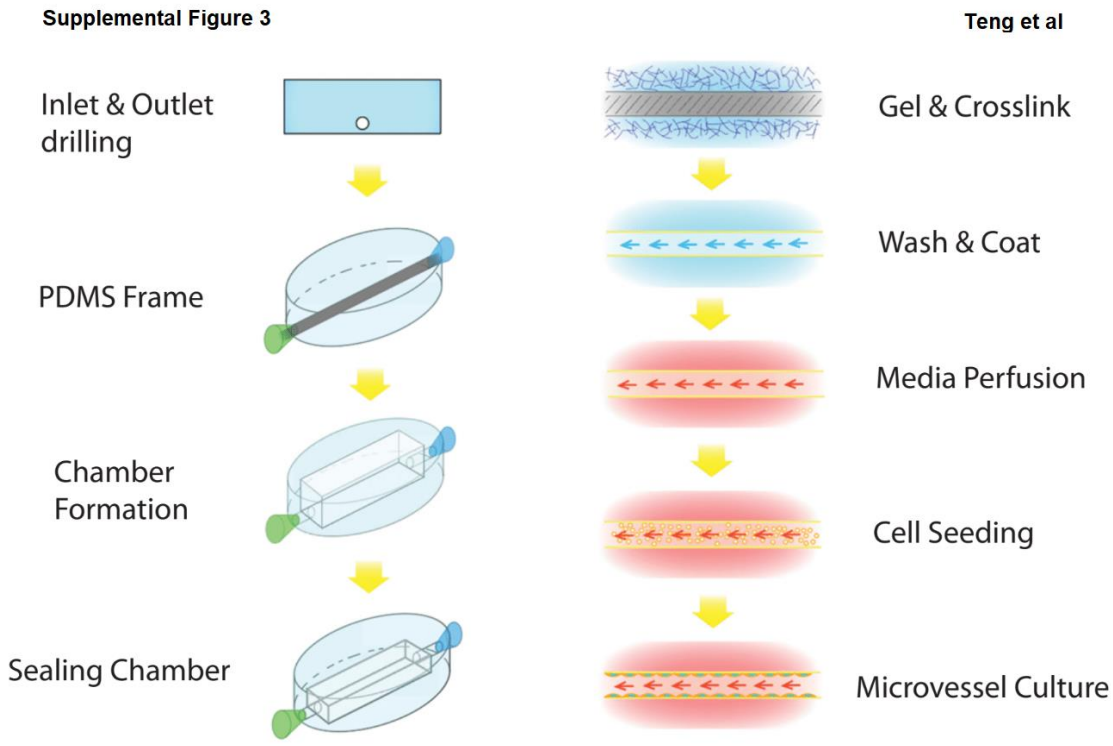

Supplementary Figure 2.3. Fabrication process of a microfluidic vessel-in-a-dish with iPSC-derived ECs
Diagram of microfluidic vessel fabrication. Device casing and framework is created first followed by matrix scaffold formation and subsequent seeding of cells for vessel formation. Components are not to scale.

Supplemental Figure 4 **Teng et al**

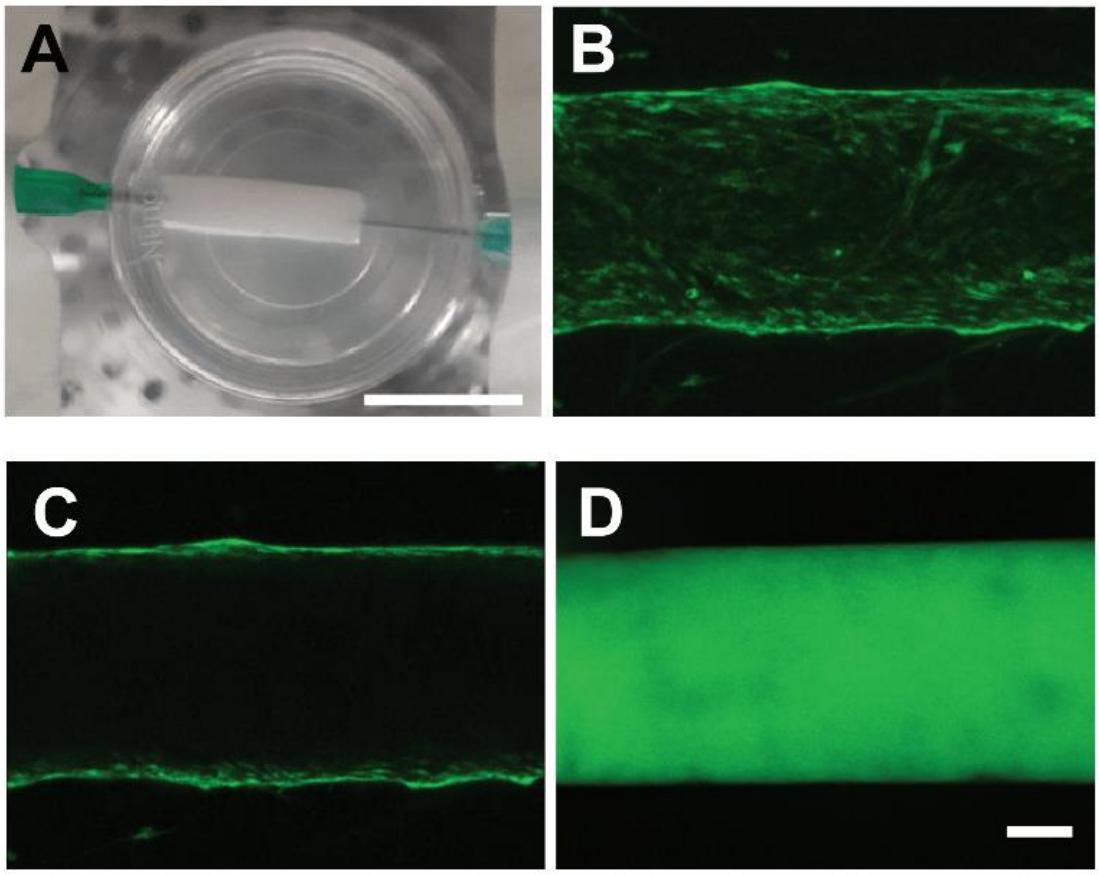

Supplementary Figure 2.4. Validation of single-channel vessel-in-a-dish with iPSC-derived ECs
(A) Image of the single-channel vessel model. Scale bar is 1 cm. Confocal imaging at the bottom (B) and midpoint (C) of the iPSC-derived EC seeded vessel shows a dense layer of cells, which form a patent vessel (D) capable of transporting a fluorescently-tagged dextran under flow. Scale bar is 100 microns.

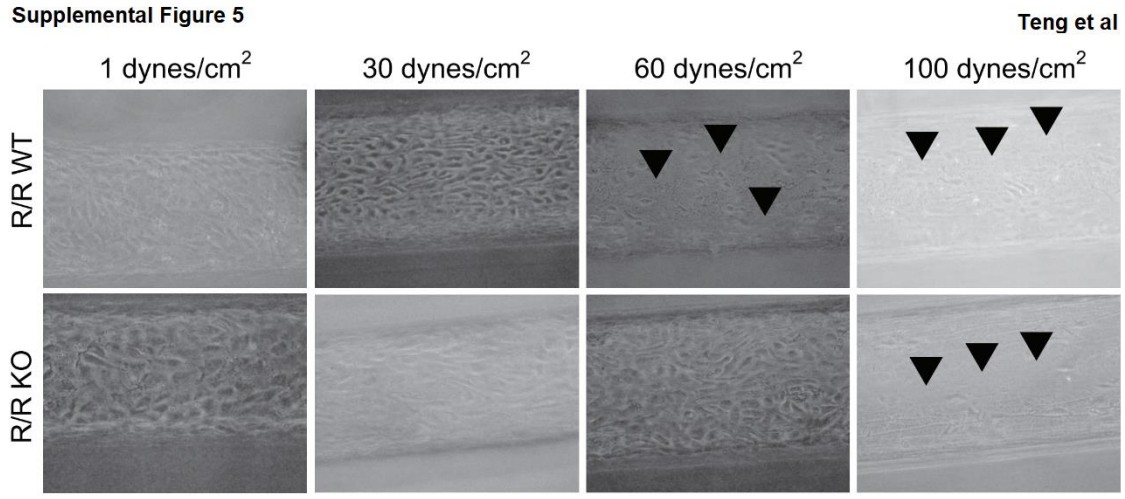

Supplementary Figure 2.5. Exposure to acute pathological shear stress preferentially detaches risk haplotype cells
Phase contrast images of vessels after 24 hours of exposure to the indicated acute shear stress. Each row of images corresponds to R/R WT (top) or KO cells (bottom). Arrowheads indicate region of cell detachment after acute shear application.

2.7 Acknowledgements

The authors would like to thank Dr. Kristen Jepsen of the Institute for Genomic Medicine (UCSD), Fyodor Urnov (Sangamo Biosciences) for design of the TALEN nucleases, and iPSCs were a generous gift from Dr. Kristin Baldwin (Scripps Research). The authors would like to thank Cody Fine, Vu Nguyen, and Elsa Molina (Sanford Consortium Stem Cell Core) for technical expertise in cell sorting and microscopy, as well as Zong Ming Chua (Sanford Burnham Prebys) for Ingenuity Pathway Analysis assistance. The authors acknowledge funding support from the National Institutes of Health (R01AG045428 to A.J.E., F32HL126406 to J.K.P.) and the National Science Foundation Graduate Research Fellowship Program (to A.K.).

Chapter 2, in full, is a reprint of the material as it appears in Teng EL, Masutani EM, Fung J, Lian R, Ngo B, Kumar A, Placone JK, Losardo V, Engler AJ. High Shear

Stress enhances Endothelial Permeability in the presence of the Risk Haplotype at 9p21.3. Submitted. The dissertation author was the primary author of this paper.

Chapter 3.

Conclusions

3.1 Introduction

The role of mechanobiology in stem cell differentiation and disease modeling has continued to be uncovered over time, but with greater advances in genetic manipulation and in-vitro modeling of tissue, the need for study of the holistic effects of genetic, environmental, and mechanical forces is growing. As had been described earlier, genetic relations to the prevalence of disease continue to grow through further study, allowing for a connection between transcriptional and functional outcomes. With recent developments in induced pluripotent stem cell genetics, these disease models can be recapitulated in a timely and economical manor in vitro. To further improve the relavence of in vitro disease modeling, environmental factors including spatial orientation and 3D cellular contact and containment introduce a more tissue like structure. Lastly, the mechanical surroundings of stretch, stiffness, and shear stress can be incorporated to induce an external stressor mimicing pathological conditions that invite activated disease progression and susceptibility. Thus, this dissertation has further explored the genetic and fluid mechanical effects on endothelial monolayer and microvessel permeability and initial coronary artery disease pathology.

3.2 Shear stress modulates CAD risk haplotype influence on endothelial function

Genome wide association studies have identified many genetic variants related to disease, but the cellular mechanisms involved with these diseases and genetic variants is not well understood. Many of these genetic risk variants contain or are within a non-coding region, which makes determining these direct effects caused by mutations or manipulation of the non-coding region difficult. In addition, disease progression can be induced by many factors which not only include genetics but environmental conditions and factors. This can be especially pertinent in disease states that experience significant mechanical stress such as myocardial infarction and coronary artery disease. To elaborate on the understanding of this disease progression, we investigated the involvement of the 9p21.3 risk haplotype in degrading endothelial cellular functionality as noted in Chapter 2. We found that endothelial monolayer showed increased permeability and reactive oxygen species generation in endothelial cells with the risk haplotype. Under shear stress, we determined endothelial microvessels of risk haplotype showed greater permeability and vessel wall detachment at lower shear stresses. The transcriptomic expression of sheared risk haplotype endothelial cells showed decreases in endothelial adhesion and ECM gene expression while showing an activated response of previously identified CAD subset genes that weren't seen in static endothelial cells. This regulation pattern

demonstrates the activation of the CAD risk region through mechanical shear stress, serving as a viable example of in-vitro disease modeling.

3.3 Future directions

The scientific studies noted in this dissertation are notable cases of disease modeling, yet further complexity and understanding can be improved on in the future. While this study illustrates the effects of endothelial dysfunction and its possible consequences related to CAD, the endothelial cell function can also influence other cells via paracrine signaling or environment effects. The progression of CAD involves smooth muscle cells as well as macrophages in the deterioration of vessel conditions, which can work in conjunction or opposition in endothelial function in pathological conditions. Further in-vitro studies would benefit greatly by introducing these cellular partners in vessel physiology in a 3D microvessel environment to understand cross-cellular interplay. In addition, the fluidic forces involved in this study were simplistic relative to the many fluidic formations possible within the body. The inquiry of the effects of pulsatile flow or turbulent flow on endothelial functionality will further extend lateral understanding relevant to greater geometries and fluidic patterns of vasculature, including vessel bifurcations and rhythmic fluid flow, respectively. Elaboration into the aforementioned details off of research dictated here can greatly further our understanding of how cell genetics, environment, and mechanical stress influences vessel health and pathology.

References

1. Tiscornia G, Vivas EL, Izpisua Belmonte JC. Diseases in a dish: modeling human genetic disorders using induced pluripotent cells. Nat Med. 2011;17(12):1570-6.

2. Liu C, Oikonomopoulos A, Sayed N, Wu JC. Modeling human diseases with induced pluripotent stem cells: from 2D to 3D and beyond. Development. 2018;145(5).

3. Sun N, Yazawa M, Liu J, Han L, Sanchez-Freire V, Abilez OJ, et al. Patient-specific induced pluripotent stem cells as a model for familial dilated cardiomyopathy. Sci Transl Med. 2012;4(130):130ra47.

4. Lian X, Zhang J, Azarin SM, Zhu K, Hazeltine LB, Bao X, et al. Directed cardiomyocyte differentiation from human pluripotent stem cells by modulating Wnt/beta-catenin signaling under fully defined conditions. Nat Protoc. 2013;8(1):162-75.

5. Patsch C, Challet-Meylan L, Thoma EC, Urich E, Heckel T, O'Sullivan JF, et al. Generation of vascular endothelial and smooth muscle cells from human pluripotent stem cells. Nat Cell Biol. 2015;17(8):994-1003.

6. Bao X, Lian X, Hacker TA, Schmuck EG, Qian T, Bhute VJ, et al. Long-term self-renewing human epicardial cells generated from pluripotent stem cells under defined xeno-free conditions. Nat Biomed Eng. 2016;1.

7. Kinney MA, Sargent CY, McDevitt TC. Temporal modulation of beta-catenin signaling by multicellular aggregation kinetics impacts embryonic stem cell cardiomyogenesis. Stem Cells Dev. 2013;22(19):2665-77.

8. Melkoumian Z, Weber JL, Weber DM, Fadeev AG, Zhou Y, Dolley-Sonneville P, et al. Synthetic peptide-acrylate surfaces for long-term self-renewal and cardiomyocyte differentiation of human embryonic stem cells. Nat Biotechnol. 2010;28(6):606-10.

9. Clause KC, Liu LJ, Tobita K. Directed stem cell differentiation: the role of physical forces. Cell Commun Adhes. 2010;17(2):48-54.

10. Discher DE, Mooney DJ, Zandstra PW. Growth factors, matrices, and forces combine and control stem cells. Science. 2009;324(5935):1673-7.

11. Zamir EA, Srinivasan V, Perucchio R, Taber LA. Mechanical asymmetry in the embryonic chick heart during looping. Ann Biomed Eng. 2003;31(11):1327-36.

12. Shradhanjali A, Riehl BD, Lee JS, Ha L, Lim JY. Enhanced cardiomyogenic induction of mouse pluripotent cells by cyclic mechanical stretch. Biochem Biophys Res Commun. 2017;488(4):590-5.

13. Du V, Luciani N, Richard S, Mary G, Gay C, Mazuel F, et al. A 3D magnetic tissue stretcher for remote mechanical control of embryonic stem cell differentiation. Nature communications. 2017;8(1):400.

14. Kurazumi H, Kubo M, Ohshima M, Yamamoto Y, Takemoto Y, Suzuki R, et al. The effects of mechanical stress on the growth, differentiation, and paracrine factor production of cardiac stem cells. PLoS One. 2011;6(12):e28890.

15. Engler AJ, Carag-Krieger C, Johnson CP, Raab M, Tang HY, Speicher DW, et al. Embryonic cardiomyocytes beat best on a matrix with heart-like elasticity: scar-like rigidity inhibits beating. J Cell Sci. 2008.

16. Jacot JG, McCulloch AD, Omens JH. Substrate stiffness affects the functional maturation of neonatal rat ventricular myocytes. Biophys J. 2008;95(7):3479-87.

17. Young JL, Engler AJ. Hydrogels with time-dependent material properties enhance cardiomyocyte differentiation in vitro. Biomaterials. 2011;32(4):1002-9.

18. Salameh A, Wustmann A, Karl S, Blanke K, Apel D, Rojas-Gomez D, et al. Cyclic mechanical stretch induces cardiomyocyte orientation and polarization of the gap junction protein connexin43. Circ Res. 2010;106(10):1592-602.

19. Ahsan T, Nerem RM. Fluid shear stress promotes an endothelial-like phenotype during the early differentiation of embryonic stem cells. Tissue Eng Part A. 2010;16(11):3547-53.

20. Cheng M, Guan X, Li H, Cui X, Zhang X, Li X, et al. Shear stress regulates late EPC differentiation via mechanosensitive molecule-mediated cytoskeletal rearrangement. PLoS One. 2013;8(7):e67675.

21. Baeyens N, Bandyopadhyay C, Coon BG, Yun S, Schwartz MA. Endothelial fluid shear stress sensing in vascular health and disease. J Clin Invest. 2016;126(3):821-8.

22. Nakayama KH, Hou L, Huang NF. Role of extracellular matrix signaling cues in modulating cell fate commitment for cardiovascular tissue engineering. Advanced healthcare materials. 2014;3(5):628-41.

23. Lippmann ES, Azarin SM, Kay JE, Nessler RA, Wilson HK, Al-Ahmad A, et al. Derivation of blood-brain barrier endothelial cells from human pluripotent stem cells. Nat Biotechnol. 2012;30(8):783-91.

24. DeStefano JG, Xu ZS, Williams AJ, Yimam N, Searson PC. Effect of shear stress on iPSC-derived human brain microvascular endothelial cells (dhBMECs). Fluids Barriers CNS. 2017;14(1):20.

25. Ikuno T, Masumoto H, Yamamizu K, Yoshioka M, Minakata K, Ikeda T, et al. Efficient and robust differentiation of endothelial cells from human induced pluripotent

stem cells via lineage control with VEGF and cyclic AMP. PLoS One. 2017;12(3):e0173271.

26. Obi S, Masuda H, Shizuno T, Sato A, Yamamoto K, Ando J, et al. Fluid shear stress induces differentiation of circulating phenotype endothelial progenitor cells. Am J Physiol Cell Physiol. 2012;303(6):C595-606.

27. Wingate K, Floren M, Tan Y, Tseng PO, Tan W. Synergism of matrix stiffness and vascular endothelial growth factor on mesenchymal stem cells for vascular endothelial regeneration. Tissue Eng Part A. 2014;20(17-18):2503-12.

28. Kong Z, Li J, Zhao Q, Zhou Z, Yuan X, Yang D, et al. Dynamic compression promotes proliferation and neovascular networks of endothelial progenitor cells in demineralized bone matrix scaffold seed. J Appl Physiol (1985). 2012;113(4):619-26.

29. Dan P, Velot E, Decot V, Menu P. The role of mechanical stimuli in the vascular differentiation of mesenchymal stem cells. J Cell Sci. 2015;128(14):2415-22.

30. Mack CP. Signaling mechanisms that regulate smooth muscle cell differentiation. Arterioscler Thromb Vasc Biol. 2011;31(7):1495-505.

31. Garcia-Cardena G, Comander J, Anderson KR, Blackman BR, Gimbrone MA, Jr. Biomechanical activation of vascular endothelium as a determinant of its functional phenotype. Proc Natl Acad Sci U S A. 2001;98(8):4478-85.

32. Humphrey JD, Dufresne ER, Schwartz MA. Mechanotransduction and extracellular matrix homeostasis. Nat Rev Mol Cell Biol. 2014;15(12):802-12.

33. Bentzon JF, Otsuka F, Virmani R, Falk E. Mechanisms of plaque formation and rupture. Circ Res. 2014;114(12):1852-66.

34. Chappell J, Harman JL, Narasimhan VM, Yu H, Foote K, Simons BD, et al. Extensive Proliferation of a Subset of Differentiated, yet Plastic, Medial Vascular Smooth Muscle Cells Contributes to Neointimal Formation in Mouse Injury and Atherosclerosis Models. Circ Res. 2016;119(12):1313-23.

35. Rensen SS, Doevendans PA, van Eys GJ. Regulation and characteristics of vascular smooth muscle cell phenotypic diversity. Neth Heart J. 2007;15(3):100-8.

36. Chopra A, Kutys ML, Zhang K, Polacheck WJ, Sheng CC, Luu RJ, et al. Force Generation via beta-Cardiac Myosin, Titin, and alpha-Actinin Drives Cardiac Sarcomere Assembly from Cell-Matrix Adhesions. Dev Cell. 2018;44(1):87-96 e5.

37. Hinson JT, Chopra A, Nafissi N, Polacheck WJ, Benson CC, Swist S, et al. HEART DISEASE. Titin mutations in iPS cells define sarcomere insufficiency as a cause of dilated cardiomyopathy. Science. 2015;349(6251):982-6.

38. Calore M, Lorenzon A, De Bortoli M, Poloni G, Rampazzo A. Arrhythmogenic cardiomyopathy: a disease of intercalated discs. Cell Tissue Res. 2015;360(3):491-500.

39. Frey N, Katus HA, Olson EN, Hill JA. Hypertrophy of the heart: a new therapeutic target? Circulation. 2004;109(13):1580-9.

40. Blaauw E, van Nieuwenhoven FA, Willemsen P, Delhaas T, Prinzen FW, Snoeckx LH, et al. Stretch-induced hypertrophy of isolated adult rabbit cardiomyocytes. Am J Physiol Heart Circ Physiol. 2010;299(3):H780-7.

41. Visel A, Zhu Y, May D, Afzal V, Gong E, Attanasio C, et al. Targeted deletion of the 9p21 non-coding coronary artery disease risk interval in mice. Nature. 2010;464(7287):409-12.

42. Kim JB, Deluna A, Mungrue IN, Vu C, Pouldar D, Civelek M, et al. Effect of 9p21.3 coronary artery disease locus neighboring genes on atherosclerosis in mice. Circulation. 2012;126(15):1896-906.

43. Soldner F, Jaenisch R. Medicine. iPSC disease modeling. Science. 2012;338(6111):1155-6.

44. Saha K, Jaenisch R. Technical challenges in using human induced pluripotent stem cells to model disease. Cell Stem Cell. 2009;5(6):584-95.

45. Park CY, Sung JJ, Choi SH, Lee DR, Park IH, Kim DW. Modeling and correction of structural variations in patient-derived iPSCs using CRISPR/Cas9. Nat Protoc. 2016;11(11):2154-69.

46. Wu H, Lee J, Vincent LG, Wang Q, Gu MH, Lan F, et al. Epigenetic Regulation of Phosphodiesterases 2A and 3A Underlies Compromised β-Adrenergic Signaling in an iPSC Model of Dilated Cardiomyopathy. Cell Stem Cell. 2015;17(1):89-100.

47. Archer CR, Sargeant R, Basak J, Pilling J, Barnes JR, Pointon A. Characterization and Validation of a Human 3D Cardiac Microtissue for the Assessment of Changes in Cardiac Pathology. Scientific reports. 2018;8(1):10160.

48. Adebayo O, Hookway TA, Hu JZ, Billiar KL, Rolle MW. Self-assembled smooth muscle cell tissue rings exhibit greater tensile strength than cell-seeded fibrin or collagen gel rings. J Biomed Mater Res A. 2013;101(2):428-37.

49. Niklason LE, Gao J, Abbott WM, Hirschi KK, Houser S, Marini R, et al. Functional arteries grown in vitro. Science. 1999;284(5413):489-93.

50. Elsayed Y, Lekakou C, Labeed F, Tomlins P. Smooth muscle tissue engineering in crosslinked electrospun gelatin scaffolds. J Biomed Mater Res A. 2016;104(1):313-21.

51. Mihalko E, Huang K, Sproul E, Cheng K, Brown AC. Targeted Treatment of Ischemic and Fibrotic Complications of Myocardial Infarction Using a Dual-Delivery Microgel Therapeutic. ACS Nano. 2018;12(8):7826-37.

52. Rufaihah AJ, Seliktar D. Hydrogels for therapeutic cardiovascular angiogenesis. Adv Drug Deliv Rev. 2016;96:31-9.

53. Wang LL, Chung JJ, Li EC, Uman S, Atluri P, Burdick JA. Injectable and protease-degradable hydrogel for siRNA sequestration and triggered delivery to the heart. J Control Release. 2018;285:152-61.

54. Zhu J, Marchant RE. Design properties of hydrogel tissue-engineering scaffolds. Expert Rev Med Devices. 2011;8(5):607-26.

55. Camci-Unal G, Annabi N, Dokmeci MR, Liao R, Khademhosseini A. Hydrogels for cardiac tissue engineering. NPG Asia Materials. 2014;6:e99.

56. Legant WR, Pathak A, Yang MT, Deshpande VS, McMeeking RM, Chen CS. Microfabricated tissue gauges to measure and manipulate forces from 3D microtissues. Proc Natl Acad Sci U S A. 2009;106(25):10097-102.

57. Hoang P, Wang J, Conklin BR, Healy KE, Ma Z. Generation of spatial-patterned early-developing cardiac organoids using human pluripotent stem cells. Nat Protoc. 2018;13(4):723-37.

58. Mills RJ, Titmarsh DM, Koenig X, Parker BL, Ryall JG, Quaife-Ryan GA, et al. Functional screening in human cardiac organoids reveals a metabolic mechanism for cardiomyocyte cell cycle arrest. Proc Natl Acad Sci U S A. 2017;114(40):E8372-E81.

59. Jackman CP, Carlson AL, Bursac N. Dynamic culture yields engineered myocardium with near-adult functional output. Biomaterials. 2016;111:66-79.

60. Ma Z, Wang J, Loskill P, Huebsch N, Koo S, Svedlund FL, et al. Self-organizing human cardiac microchambers mediated by geometric confinement. Nature communications. 2015;6:7413.

61. Shadrin IY, Allen BW, Qian Y, Jackman CP, Carlson AL, Juhas ME, et al. Cardiopatch platform enables maturation and scale-up of human pluripotent stem cell-derived engineered heart tissues. Nature communications. 2017;8(1):1825.

62. Mathur A, Loskill P, Shao K, Huebsch N, Hong S, Marcus SG, et al. Human iPSC-based cardiac microphysiological system for drug screening applications. Scientific reports. 2015;5:8883.

63. Gheorghiade M, Bonow RO. Chronic heart failure in the United States: a manifestation of coronary artery disease. Circulation. 1998;97(3):282-9.

64. Okrainec K, Banerjee DK, Eisenberg MJ. Coronary artery disease in the developing world. Am Heart J. 2004;148(1):7-15.

65. Deloukas P, Kanoni S, Willenborg C, Farrall M, Assimes TL, Thompson JR, et al. Large-scale association analysis identifies new risk loci for coronary artery disease. Nat Genet. 2013;45(1):25-33.

66. Hershberger RE, Hedges DJ, Morales A. Dilated cardiomyopathy: the complexity of a diverse genetic architecture. Nat Rev Cardiol. 2013;10(9):531-47.

67. Harismendy O, Notani D, Song X, Rahim NG, Tanasa B, Heintzman N, et al. 9p21 DNA variants associated with coronary artery disease impair interferon-gamma signalling response. Nature. 2011;470(7333):264-8.

68. Congrains A, Kamide K, Oguro R, Yasuda O, Miyata K, Yamamoto E, et al. Genetic variants at the 9p21 locus contribute to atherosclerosis through modulation of ANRIL and CDKN2A/B. Atherosclerosis. 2012;220(2):449-55.

69. O'Bleness M, Searles VB, Varki A, Gagneux P, Sikela JM. Evolution of genetic and genomic features unique to the human lineage. Nat Rev Genet. 2012;13(12):853-66.

70. Dutta A, Henley W, Lang IA, Murray A, Guralnik J, Wallace RB, et al. The coronary artery disease-associated 9p21 variant and later life 20-year survival to cohort extinction. Circ Cardiovasc Genet. 2011;4(5):542-8.

71. Lo Sardo V, Chubukov P, Ferguson W, Kumar A, Teng EL, Duran M, et al. Unveiling the Role of the Most Impactful Cardiovascular Risk Locus through Haplotype Editing. Cell. 2018;175(7):1796-810 e20.

72. Kumar A, Thomas SK, Wong KC, Lo Sardo V, Cheah DS, Hou YH, et al. Mechanical activation of noncoding-RNA-mediated regulation of disease-associated phenotypes in human cardiomyocytes. Nat Biomed Eng. 2019;3(2):137-46.

73. Durieux R, Van Damme H, Labropoulos N, Yazici A, Legrand V, Albert A, et al. High prevalence of abdominal aortic aneurysm in patients with three-vessel coronary artery disease. Eur J Vasc Endovasc Surg. 2014;47(3):273-8.

74. Hansson GK. Inflammation, atherosclerosis, and coronary artery disease. N Engl J Med. 2005;352(16):1685-95.

75. Herrmann J, Lerman A. The endothelium: dysfunction and beyond. Journal of nuclear cardiology : official publication of the American Society of Nuclear Cardiology. 2001;8(2):197-206.

76. LaMack JA, Friedman MH. Individual and combined effects of shear stress magnitude and spatial gradient on endothelial cell gene expression. Am J Physiol Heart Circ Physiol. 2007;293(5):H2853-9.

77. Marcos-Ramiro B Fau - García-Weber D, García-Weber D Fau - Millán J, Millán J. TNF-induced endothelial barrier disruption: beyond actin and Rho. (2567-689X (Electronic)).

78. Chiu J-J, Chien S. Effects of Disturbed Flow on Vascular Endothelium: Pathophysiological Basis and Clinical Perspectives. Physiological Reviews. 2011;91(1):327-87.

79. Zhou J, Li YS, Chien S. Shear stress-initiated signaling and its regulation of endothelial function. (1524-4636 (Electronic)).

80. Fisher AB, Chien S Fau - Barakat AI, Barakat Ai Fau - Nerem RM, Nerem RM. Endothelial cellular response to altered shear stress. (1040-0605 (Print)).

81. Helgadottir A, Thorleifsson G, Manolescu A, Gretarsdottir S, Blondal T, Jonasdottir A, et al. A common variant on chromosome 9p21 affects the risk of myocardial infarction. Science. 2007;316(5830):1491-3.

82. McPherson R, Pertsemlidis A, Kavaslar N, Stewart A, Roberts R, Cox DR, et al. A common allele on chromosome 9 associated with coronary heart disease. Science. 2007;316(5830):1488-91.

83. Samani NJ, Erdmann J, Hall AS, Hengstenberg C, Mangino M, Mayer B, et al. Genomewide association analysis of coronary artery disease. N Engl J Med. 2007;357(5):443-53.

84. Sutera SP, Skalak R. The history of Poiseuille's law. Annual Review of Fluid Mechanics. 1993;25:1-19.

85. Oyre S, Ringgaard S, Kozerke S, Paaske WP, Erlandsen M, Boesiger P, et al. Accurate noninvasive quantitation of blood flow, cross-sectional lumen vessel area and wall shear stress by three-dimensional paraboloid modeling of magnetic resonance imaging velocity data. J Am Coll Cardiol. 1998;32(1):128-34.

86. Fung Y-C. Biomechanics: Circulation. 2nd ed: Springer; 1997.

87. Samady H, Eshtehardi P, McDaniel MC, Suo J, Dhawan SS, Maynard C, et al. Coronary artery wall shear stress is associated with progression and transformation of atherosclerotic plaque and arterial remodeling in patients with coronary artery disease. Circulation. 2011;124(7):779-88.

88. Nikpay M, Goel A, Won HH, Hall LM, Willenborg C, Kanoni S, et al. A comprehensive 1,000 Genomes-based genome-wide association meta-analysis of coronary artery disease. Nat Genet. 2015;47(10):1121-30.

89. Howson JMM, Zhao W, Barnes DR, Ho WK, Young R, Paul DS, et al. Fifteen new risk loci for coronary artery disease highlight arterial-wall-specific mechanisms. Nat Genet. 2017;49(7):1113-9.

90. van der Harst P, Verweij N. Identification of 64 Novel Genetic Loci Provides an Expanded View on the Genetic Architecture of Coronary Artery Disease. Circ Res. 2018;122(3):433-43.

91. Larson MG, Atwood LD, Benjamin EJ, Cupples LA, D'Agostino RB, Sr., Fox CS, et al. Framingham Heart Study 100K project: genome-wide associations for cardiovascular disease outcomes. BMC medical genetics. 2007;8 Suppl 1:S5.

92. Jarinova O, Stewart AF, Roberts R, Wells G, Lau P, Naing T, et al. Functional analysis of the chromosome 9p21.3 coronary artery disease risk locus. Arterioscler Thromb Vasc Biol. 2009;29(10):1671-7.

93. Gutierrez E, Flammer AJ, Lerman LO, Elizaga J, Lerman A, Fernandez-Aviles F. Endothelial dysfunction over the course of coronary artery disease. Eur Heart J. 2013;34(41):3175-81.

94. Beckie TM, Beckstead JW, Groer MW. The association between variants on chromosome 9p21 and inflammatory biomarkers in ethnically diverse women with coronary heart disease: a pilot study. Biol Res Nurs. 2011;13(3):306-19.

95. Deanfield JE, Halcox JP, Rabelink TJ. Endothelial function and dysfunction: testing and clinical relevance. Circulation. 2007;115(10):1285-95.

96. Kinlay S, Ganz P. Role of endothelial dysfunction in coronary artery disease and implications for therapy. Am J Cardiol. 1997;80(9A):11I-6I.

97. Quillard T, Araujo HA, Franck G, Shvartz E, Sukhova G, Libby P. TLR2 and neutrophils potentiate endothelial stress, apoptosis and detachment: implications for superficial erosion. Eur Heart J. 2015;36(22):1394-404.

98. Cooper DN, Krawczak M, Polychronakos C, Tyler-Smith C, Kehrer-Sawatzki H. Where genotype is not predictive of phenotype: towards an understanding of the molecular basis of reduced penetrance in human inherited disease. Hum Genet. 2013;132(10):1077-130.

99. Ondeck MG, Kumar A, Placone JK, Plunkett CM, Matte BF, Wong KC, et al. Dynamically stiffened matrix promotes malignant transformation of mammary epithelial cells via collective mechanical signaling. Proc Natl Acad Sci U S A. 2019;116(9):3502-7.

100. Stowers RS, Allen SC, Sanchez K, Davis CL, Ebelt ND, Van Den Berg C, et al. Extracellular Matrix Stiffening Induces a Malignant Phenotypic Transition in Breast Epithelial Cells. Cell Mol Bioeng. 2017;10(1):114-23.

101. Segel M, Neumann B, Hill MFE, Weber IP, Viscomi C, Zhao C, et al. Niche stiffness underlies the ageing of central nervous system progenitor cells. Nature. 2019;573(7772):130-4.